ABSTRACT

DEVELOPMENT, TESTING, AND NUMERICAL MODELING OF A FOAM SANDWICH BIOCOMPOSITE

By

Kyle E. Chan

May 2014

This study develops a novel sandwich composite material using plant based materials for potential use in nonstructural building applications. The face sheets comprise woven hemp fabric and a sap based epoxy, while the core comprises castor oil based foam with waste rice hulls as reinforcement. Mechanical properties of the individual materials are tested in uniaxial compression and tension for the foam and hemp, respectively. The sandwich composite is tested in 3 point bending. Flexural results are compared to a finite element model developed in the commercial software Abaqus, and the validated model is then used to investigate alternate sandwich geometries. Sandwich model responses are compared to existing standards for non-structural building panels, showing that the novel material is roughly half the strength of equally thick drywall. When space limitations are not an issue, a double thickness sandwich biocomposite is found to be a structurally acceptable replacement for standard gypsum drywall.

DEVELOPMENT, TESTING, AND NUMERICAL MODELING OF A FOAM SANDWICH BIOCOMPOSITE

A THESIS

Presented to the Department of Civil Engineering and
Construction Engineering Management

California State University, Long Beach

In Partial Fulfillment

of the Requirements for the Degree

Master of Science in Civil Engineering

Committee Members:

Yu-Fu Ko, Ph.D. (Chair)
Sergio Mendez, Ph.D.
Lisa Star, Ph.D.

College Designee:

Antonella Sciortino, Ph.D.

By Kyle E. Chan

B.S., 2010, University of California, Los Angeles

May 2014

ProQuest LLC.
789 East Eisenhower Parkway
P.O. Box 1346
Ann Arbor, MI 48106 - 1346

ACKNOWLEDGEMENTS

I would like to thank my entire thesis committee for their ongoing support of this project. In particular, I want to thank Dr. Ko for being involved with every research project I have worked on since coming to CSULB. He connected me with the opportunities I needed to really excel in this program rather than becoming just another number.

I would also like to thank Ignacio Cervantes and Lisa AungYong for all their help. Ignacio expedited my learning to use Abaqus, and mentored me through the use of the various testing equipment in the structures lab. Lisa AungYong worked alongside me on this project, led the material fabrication process, and brought the chemical expertise necessary to make the foam development actually possible.

For funding this project, I would like to thank California State University, Long Beach for awarding the 2013-2014 Multidisciplinary Research Award to Drs. Ko and Mendez.

Finally, I want to thank my parents, Sam and Ginny Chan, who supported me endlessly, and gave me the boosts I needed when times were rough. My sister, Amy Chan, always gave me a reason to feel positive about things. And of course, my girlfriend, Michelle Ho, stuck with me and kept pushing me to succeed all these years. They were all instrumental in getting me here, and I am thankful for their support.

TABLE OF CONTENTS

LIST OF TABLES

TABLE Page

LIST OF FIGURES

FIGURE Page

FIGURE Page

CHAPTER 1

INTRODUCTION

This study aims to develop and test a new sandwich composite board using renewable green materials. The foam core will use a castor-oil based polymer and will utilize spent rice hulls for reinforcement, while the face plates will use woven hemp fibers embedded in a tree sap-based epoxy. A numerical model will also be developed to check additional geometric configurations.

Composites use a combination of different materials in such a way that the strengths of one material can support the weaknesses of the others. Simple composite laminates use strong fibers to withstand tensile loads coupled with a polymer matrix, such as epoxy, to resist bending and support the material under compression. Sandwich composites of the type considered here are composed of a lightweight core sandwiched between two stiff laminate face sheets. These materials have great strength to weight ratios, with the core carrying the shear stresses while the face sheets carry the flexural stresses.

While these materials can be made extremely strong, they often utilize many synthetic materials. Such materials are often expensive to produce, create hazardous conditions for workers during production, and must be carefully disposed of to avoid damage to the environment. Plant-based materials are generally cheaper and much less hazardous to both humans and the environment, but exhibit limited strength compared to

their synthetic counterparts. The plant-based materials used in this sandwich biocomposite are hemp fiber, tree sap, spent rice hulls, and castor oil.

A primary goal of this study will be to maximize the use of these natural materials without sacrificing significant material strength. The materials will be tested both for their individual strengths in tension and compression and for the overall sandwich's strength in 3-point flexure.

A finite element model of the sandwich beam using the individual material property data will be developed and compared to the experimental results for the sandwich beam in flexure. Once the model is determined to be reasonably accurate, additional geometries will be tested to compare the material strengths to building code requirements for various non-structural building panels.

The findings of this study will aid future research regarding biocomposites in civil structures. Additionally, if this new material can be built to satisfy building code strength requirements, it may be a viable alternative to gypsum drywall for non-load bearing structural panels.

CHAPTER 2

BACKGROUND AND REVIEW OF PREVIOUS RESEARCH

Polymeric Foams

Polymeric foams generally progress through three distinct stages during loading (Figure 1). In the first stage, the foam behaves linearly elastically. In the second, the cell walls begin to plastically deform, creating a plateau where the stress remains constant as the strain continues increasing. Finally, the foam enters a densification region as the cells completely collapse and opposing cell walls are braced directly against each other. Thus, foam strength is directly related to its density. Increased density leads to greater elastic modulus and yield stress, although the densification region starts at smaller strains (Fereidoon and Taheri 2012). However, denser foams can actually be less effective at absorbing impact energy because the strain may not reach the stress plateau, causing unnecessary forces from the rapid deceleration.

The strength of polymeric foams can also be noticeably dependent on strain rate and temperature (Zhang et al. 1997). Increased strain rates, such as those involved during impact loading, can lead to increased stiffness and strength responses. Conversely, increased temperature during loading tends to reduce the material strength.

Strain rate effects were also investigated during an in-depth study on Rohacell-51WF, a specific type of polymeric foam (Li et al. 2000). This study confirmed that increased strain rate leads to increased compressive failure stress, but additional tests

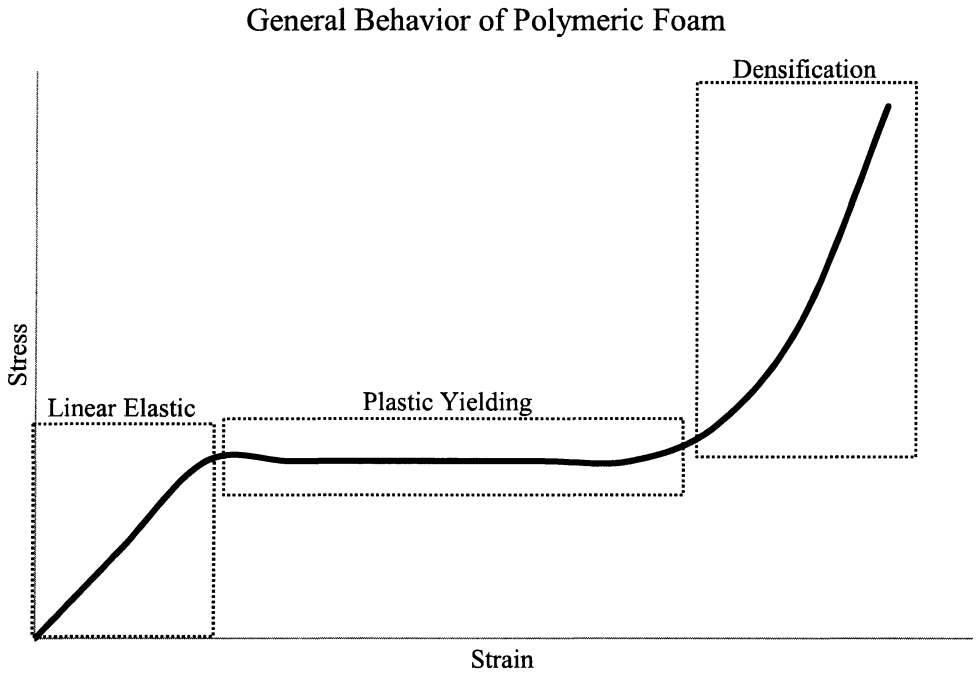

FIGURE 1: General foam behavior.

showed that strain rate has minimal effects on shear failure stress until very high strain rates, at which point the strength actually decreased. The tests performed also included hydrostatic compression and compression with simultaneous shear, two tests that require more specialized equipment than will be available for this study. Results from the latter test showed that compression damage can lead to noticeable reductions in shear strength. Across all the performed tests, the authors found that the various stress ranges (compression, tension, and shear) behaved very differently, and therefore stressed the importance of differentiating between them in a foam material model, whether analytical or numerical.

Various studies have shown that introducing small particles or fibers into a foam improves its material properties. One such study found that nanoparticles dispersed

throughout a polyurethane foam increased the mechanical strength while also decreasing its thermal degradation (Saha et al. 2008). These nanoparticles were even more effective than more conventional microparticles due to their much greater surface area and surface energy. Another study on the effect of adding fiber reinforcement to concrete foam found additional benefits for a normally brittle material (Flores-Johnson and Li 2012). The fiber reinforcement greatly increased the foam's ductility, allowing even the brittle concrete to enter a densification region at high strains. However, the stronger foam also changed the composite's ultimate failure mode to a more brittle one, leading the authors to recommend a higher factor of safety when working with such materials. This is considered in the present study when adding small particles to the foam mixture.

Fiber Reinforced Polymer Composite Laminates

Fiber-reinforced polymer (FRP) composite laminates exhibit varying strengths and stiffnesses depending on the alignment between the fibers and the loading direction. Researchers found that tensile strength is greatest at 0° (fibers are perfectly aligned with the loading), and quickly drops off to a relative constant beyond 15° (Hassan and Batra 2008). Additionally, fibers aligned at 45° showed the highest strain at failure. By stacking multiple layers of fiber at different angles, the transversely isotropic material can be treated as fully orthotropic. The present study utilizes this property of composite laminates to both maximize the material's strength and simplify the finite element model.

Sandwich Composites

Sandwich composites like the one developed here are an effective way to create lightweight materials for supporting flexural loads. The general structure of a sandwich composite is a lightweight core material sandwiched between two face sheets. The face

sheets tend to be fairly stiff and strong materials such as steel plate or composite laminate. The core is a lightweight material such as foam, plywood, or cardboard, and therefore tends to be relatively weak. By separating and supporting the much stiffer face sheets, however, the core increases the second moment of area for the beam or plate, augmenting its flexural strength. Additionally, the low density core increases the specific strength of the composite by decreasing its density.

An early work on sandwich composite beams created simple elastic-plastic models that worked reasonably well (Mines and Jones 1995). The authors assumed a progressive failure consisting of 3 steps. First the upper skin would fail by compression, creating a plastic hinge, followed by core crushing and finally lower skin tensile failure. Experimental results confirmed this assumption, but the beam was intentionally made to follow certain geometry restrictions to avoid unwanted failure types. The results also showed a difference in failure mechanisms between the bottom (tensile) face of the sandwich beam and the laminate material in the pure tension test.

Further studies explored the initial failure modes exhibited by sandwich beams loaded in 3 point bending. These primary failure modes are microbuckling of the top face sheet, face wrinkling, core shear failure, and local indentation at the loading point (Steeves and Fleck 2004a). Steeves and Fleck developed an analytical model that, given a specified ratio of core strength to face sheet strength, could create a metric showing the most likely initial failure mode according to the sandwich beam's relative geometry (Figure 2). This failure mode map uses the non-dimensional parameters $\bar{t}$ and $\bar{c}$ for its axes, and is unique to a particular combination of $\bar{\sigma}^2\bar{E}$ and $\bar{\tau}$. These parameters are defined as follows.

$$\bar{t} = t_f/c \tag{3.1}$$

$$\bar{c} = c/L \tag{3.2}$$

$$\bar{\sigma} = \sigma_c/\sigma_f \tag{3.3}$$

$$\bar{\tau} = \tau_c/\sigma_f \tag{3.4}$$

$$\bar{E} = E_f/\sigma_f \tag{3.5}$$

Where:

c = Core thickness

t_f = Face sheet thickness

L = Beam length

σ_c = Core crushing strength

σ_f = Face sheet microbuckling strength

τ_c = Core shear strength

E_f = Face sheet axial modulus

In short, the failure mode map assumes certain ratios of material strengths and determines the most likely initial failure mode according to the particular geometry of the beam. In general, core shear failure was observed in beams with thick faces and small spans, face microbuckling occurred in long beams with dense cores and thin faces, and indentation occurred in long beams with weak cores and thin faces.

An expansion on the conclusions of Steeves and Fleck (2004a) tested similar beams in 3 point bending with the ends fixed rather than pinned (Tagarielli et al. 2004). The results showed that the beam response was heavily affected by the support

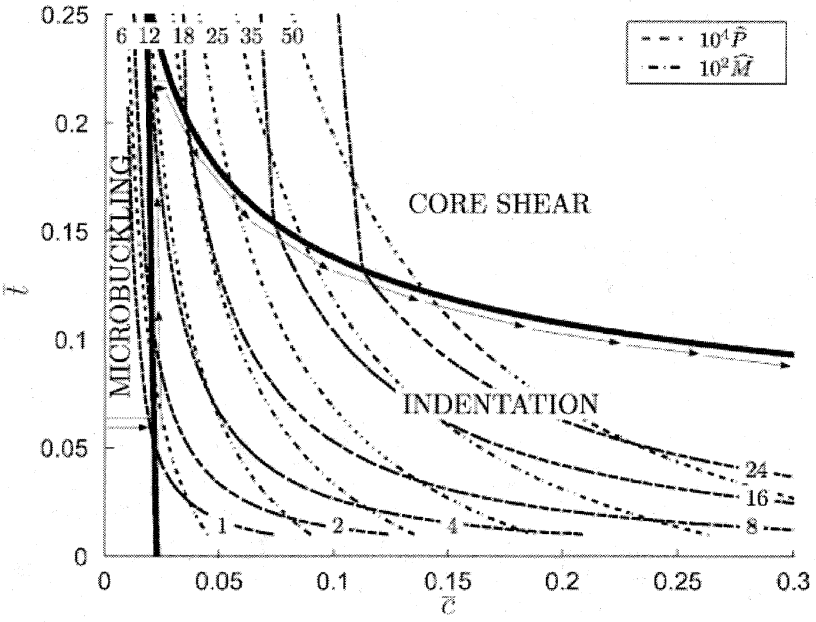

FIGURE 2: Failure mode map of a foam sandwich beam (Steeves and Fleck 2004a).

conditions. The fixed beam almost never failed from microbuckling because the top face was not in compression, and it exhibited a hardening effect after initial yield.

In an experimental study comparing sandwich beams composed of various face sheet laminates and core foams, it was found that the core type has a greater effect on the beam's strength than the face sheet (Mamalis et al. 2008). Elastic foams displayed greater strength and energy absorption than their more rigid counterparts. The improved energy absorption was caused by the elastic foams failing in local indentation, which steadily carried more load after initial failure, compared to rigid foams failing in shear which saw a sudden drop in load capacity after initial failure. Core shear failure, in general, is an undesirable failure mode because of its rigidity and energy absorbing inefficiency (Lim

et al. 2004). Thus, the present study utilizes more elastic foams for the core material in an attempt to avoid core shear failure.

Finite Element Modeling

There are many theoretical models that can be used to computationally model composite laminates and sandwiches (Kreja 2011). These range from Equivalent Single Layer models that homogenize the material into a single layer, to Discrete Layer models that look at each layer separately. Additionally, some 3D models combine different methods for different areas of the laminate. These techniques are necessary because micromechanical analysis is too computationally expensive for most practical applications.

A finite element model relies heavily on material data provided to the program to accurately predict the material responses. However, by its nature, finite element analysis is an approximate solution method. More data is usually better, but it is generally not feasible to perfectly model every material. Simplifying assumptions are required to keep computation times within a reasonable limit, and often a study will neither have access to certain material properties nor have the capability to obtain them through testing. The next few studies make varying simplifications to their finite element material models and investigate the effects of these simplifications on their results.

Borsellino et al. (2004) studied a multilayered sandwich structure with intermediate layers of denser foam between the core foam and the fiber face sheets (Borsellino et al. 2004). All the materials were simplified as fully elastic, which caused the numerical results to deviate greatly from the experimental results after the point of failure (Figure 3). However, the results up to that point were reasonably accurate.

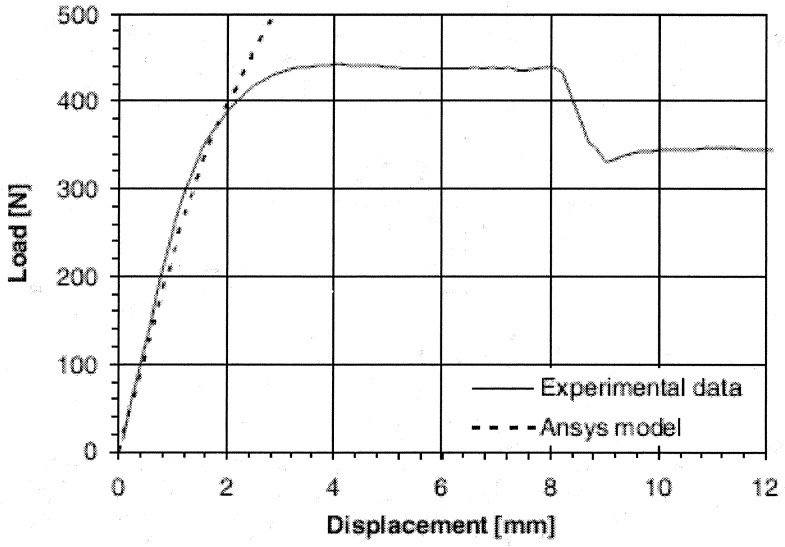

FIGURE 3: Load-displacement curve for a fully elastic finite element model. (Borsellino et al. 2004).

Around the same time, Steeves and Fleck (2004b) developed a numerical model in Abaqus for sandwich beams in 3 point bending (Steeves and Fleck 2004b). They used a previously developed user material subroutine (UMAT) to model the foam damage, and modeled the face sheets as perfectly elastic and orthotropic. Their results agreed reasonably well with the experimental results, and gave a slightly better representation of failure than their analytical model (Figure 4). The overall results were consistently slightly stronger than the experimental results, which may be attributed to the lack of damage criteria for the face sheets.

In high speed impact tests, modeling the foam crushing behavior is vital in creating an accurate failure model (Ivañez et al. 2010). Rather than modeling the face sheets as 2D planes, they were modeled as 3D solids and used a dynamic user material subroutine (VUMAT) to prescribe the Hou laminar composite failure criterion. The foam

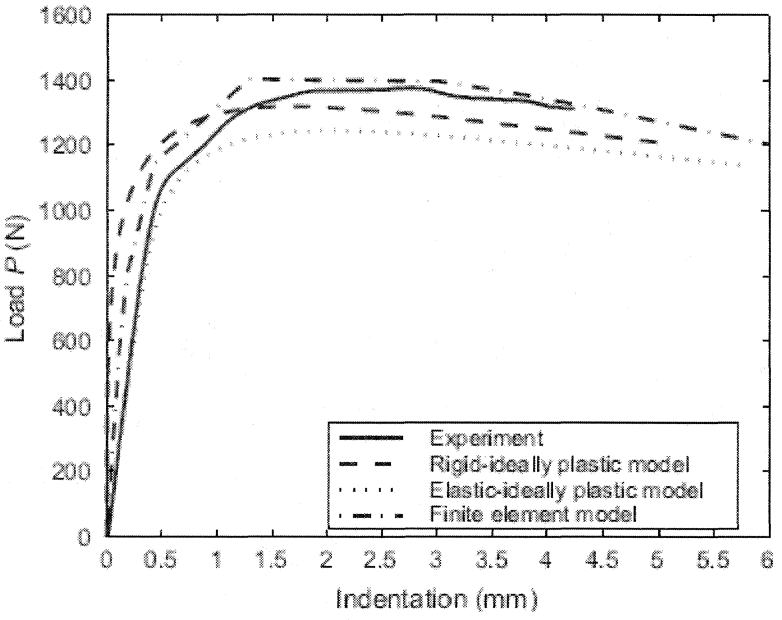

FIGURE 4: Load-displacement curve for a sandwich model with elastic face sheets and plastic deformable foam. (Steeves and Fleck 2004b).

was modeled first by the built-in Crushable Foam model in Abaqus, and second as a purely elastic solid. Compared to the experimental results, the crushable foam model produced reasonable results in both deformation and energy absorption. However, removing the crushing characteristic of the foam reduced the chance for local indentation and subsequently led the beam model to fail at a much greater load.

Another study investigated the importance of modeling damage for a sandwich beam under local indentation loading (Rizov 2008). The authors applied a custom failure criterion to the face sheets that determined when the element failed, at which point that element's material parameters were reduced by a factor of 1000. The foam was modeled using the built-in crushable foam model. The beam was modeled in 2D plane strain. By comparing their model to a similar one with purely elastic face sheets (similar to those

used by Steeves and Fleck (2004b)), they found that at smaller indentations the two models agreed reasonably well, but after a certain point the linear elastic model began to overestimate the beam's strength and underestimate the residual dent in the surface upon unloading (Figure 5). Since the present study's analysis investigates nonlinear failure of the beam, it must consider the plastic behaviors of both the foam (crushing) and the face sheets (progressive failure).

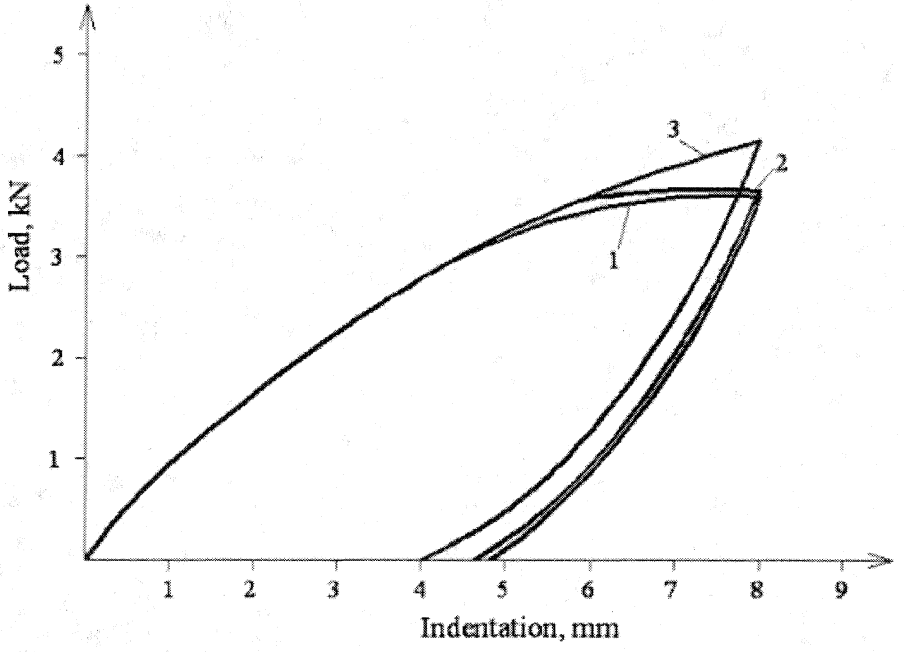

FIGURE 5: Sandwich beam local indentation curve comparison. Showing experimental data (curve 1), FEM results including face sheet damage (curve 2), and FEM results neglecting face sheet damage (curve 3). (Rizov 2008).

One of the required parameters in Abaqus's Crushable Foam material model is the ratio of yield stress in hydrostatic tension to initial yield stress in hydrostatic compression (Dassault Systèmes 2010). As both of these values, particularly hydrostatic tension, are

quite difficult to test, Abaqus recommends assuming a value of 10% for this ratio. However, this assumption is often inaccurate when any large tensile stresses are involved (Li et al. 2000). Fortunately, the dominating stresses in a sandwich beam's core are generally compressive in nature; modifying this ratio should minimal effect on the outcome of the simulation (Mines and Alias 2002). This study uses this assumption when constructing the finite element model, verifying its validity once the model is completed.

Biocomposites

Natural fibers can be classified as either plant-based or animal-based fibers. Plant-based fibers can be further divided according to their source as either primary or secondary plants (Faruk et al. 2012). Primary plants, including jute and hemp, are grown for their fiber content. Secondary plants include rice and pineapple, from which the fiber is produced as a by-product. While there are environmental advantages to using plant fibers in composite materials, plant fibers tend to be hydrophilic, which can cause problems in interactions with the rest of the material, particularly the polymer matrix (La Mantia and Morreale 2011). In general, adding plant fibers causes an increase in stiffness and flexural strength but a decrease in ductility compared to the plain matrix material.

Fully green composites are those materials that can be cleanly disposed of or recycled at the end of their life cycle, but often at the cost of material strength (John and Thomas 2008). Hybrid composites seek a middle ground, using synthetic materials for increased strength while still using biomaterials for their lower environmental impact. This study aims to use both primary (hemp) and secondary (rice hulls) plants in combination with some synthetic polymers to create a hybrid material. This should

maximize the renewability of the composite while retaining the strength and ductility of the synthetic polymers.

Research regarding the use of biocomposites in structural applications is already underway. In one study, rigid boards were fabricated using hemp or flax fibers embedded in polyester resin, and their strength was compared to standard building floor materials such as prestressed concrete slabs and hollow core concrete slabs (Burgueño et al. 2005). The results showed the biocomposites to be comparable in strength to the prestressed concrete slabs, and were an acceptable replacement for conventional housing panels according to international building code requirements.

While there have been many studies on biocomposite materials in general, most of them utilize chemically treated fibers or hybrid composites (Jawaid and Abdul Khalil 2011). Additionally, this research is spread out over the wide range of natural fibers and their various applications, so the particular case of hemp laminates in a sandwich beam has very little exposure. One study investigated a sandwich material that used chopped hemp fibers for the core material as well as woven hemp fabric as the skin (Kabir et al. 2012). The focus of this study was on the chemical treatment of the hemp fibers, and showed that the mechanical strength of natural fiber composites is largely governed by the strength of the fiber-matrix bond. However, there has been very little research on biocomposites with minimal chemical treatment, and among those even fewer that investigate potential applications for such materials. Thus, the present study not only presents a novel material, but also contributes to the rapidly growing development of biocomposite materials in a relatively unexplored area.

CHAPTER 3

PROBLEM STATEMENT

Modern construction materials are generally chosen for their mechanical properties, cost efficiency, and appearance. Materials such as concrete, steel, timber, and drywall have been through extensive testing leading to a well established knowledge of their material properties. Additionally, their widespread use allows facilities to specialize in specific types of materials, which lowers production costs and standardizes their appearance. Despite these advantages, however, there is a growing need for sustainability in the construction industry. Conventional building materials do not utilize waste sources adequately, if at all, while their production and disposal methods often have negative effects on the environment in the form of air pollution or deforestation. Many avenues exist for increasing the sustainability of such materials, but one in particular that is focused on here is the development of biocomposites.

Biocomposites utilize natural, often plant-based, fibers in a polymer resin to create a material that is comparable in strength to a similar synthetic material. These materials are often biodegradable and renewable due to their components coming from easily farmed crops and animals. Although there has been much research in the area of biocomposites, it is still a relatively new field. Most biocomposite production techniques require the use of potentially hazardous chemicals for pretreatment of the plant fibers, and hybrid composites are often the standard for biocomposites. These hybrid techniques

provide increased sustainability over their purely synthetic counterparts, but there are many avenues for improvement in this area. This study aims to minimize the use of synthetic or hazardous materials during production, as well as utilizing waste sources that would otherwise be untapped.

The problem, and its solution, is twofold. The first part is the utilization of waste materials. As the name suggests, these materials are most often disposed of as waste products rather than being reused for material fabrication. For example, in Northern California alone, 360,000 tons of waste rice hulls are produced, and 200,000 tons are burned as fuel in power plants (Mendez and Ko 2013). The leftover silica ashes as well as the unburned hulls are simply disposed of in landfills or other waste disposal sites. These waste products represent an untapped resource for material reinforcements in many industries, including civil engineering.

The second part is that the construction industry is somewhat slow in introducing green building materials to various infrastructure projects. There is a dearth of research regarding civil engineering applications of biocomposite materials, and the industry sees rather limited use of laminate or sandwich composites in general. This lethargy might be attributed to the construction standards that require thorough testing and study before introducing new materials or methods to the system. Such a necessity tends to delay innovations from widespread use.

This study addresses the first problem by utilizing spent rice hulls as reinforcement in the foam. Provided the organic material does not negatively impact the foaming chemistry, this method will utilize a waste material and improve both the overall composite's sustainability and its material strength. The second problem is addressed

through analysis of the new material for potential non-structural applications in civil building design. Any data acquired here, whether positive or negative, will help move the industry toward more sustainable practices in design and construction.

CHAPTER 4

METHODOLOGY

The goals of this study were achieved through three overarching steps. First, the base materials were fabricated and tested. Various foam types were tested to determine the optimal foam for the sandwich. Second, the sandwich composite was fabricated and tested using the best foam and the hemp laminate. All material testing was performed on the Tinius Olsen Super L Universal Testing Machine in the CSULB Highway and Structures laboratory. Finally, a finite element model of the sandwich composite was created using the commercial program Abaqus, and was used to compare the sandwich composite to commercial drywall.

Materials

Hemp Laminate

The sandwich face sheets were made by vacuum infusing an epoxy resin into a woven fiber cloth. The cloth used was a 12.5 oz. woven hemp fabric purchased from Pickering International. The resin was SuperSap, a proprietary resin produced by Entropy Resins, Inc. that the manufacturers claim derives at least 50% of its volume from tree sap. These materials were chosen because they utilize renewable, natural resources. Additionally, hemp fiber is one of the strongest plant fibers available, and has seen extensive use as rope and fabric material throughout human history.

The face sheet was constructed from two sheets of fabric. The first sheet was cut straight so the fibers were positioned at 0°/90°, while the second was cut at an angle so the fibers were positioned at 45°/45°. These sheets were then stacked and placed on a steel plate that had been coated with a non-stick spray. This plate ensured that the laminate would remain flat during the vacuum infusion process. Two more layers of fabric were then placed on top of the hemp: first a no-stick fabric to ensure the hemp would not adhere to the vacuum bag, and then a plastic mesh fabric to create voids that the vacuum could pull the resin through (Figure 6). All of these layers were temporarily glued together by Airtech EconoTac 2, a weak spray adhesive, during the layup process.

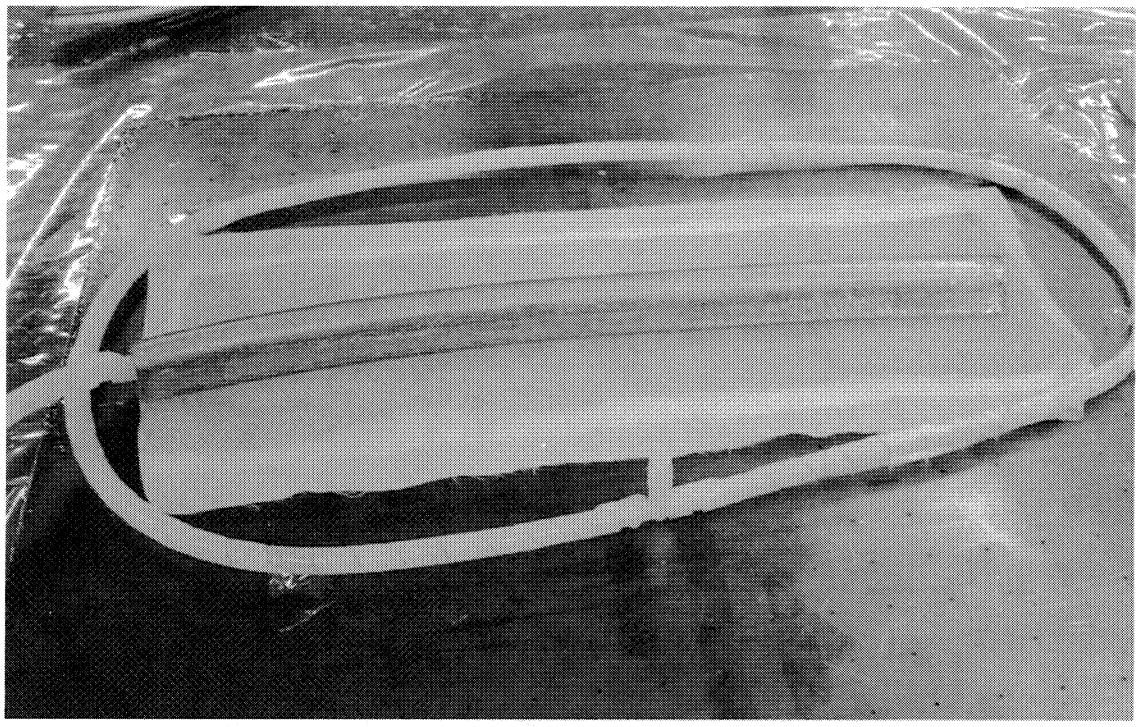

FIGURE 6: Pre-bagging layup of the hemp laminate. Showing the mesh (top layer), non-stick fabric (2nd layer), steel plate, slotted hoses, and cable cover.

This layup was sealed in a plastic bag with one slotted hose lining the perimeter and a second slotted hose across the center of the fabric. The center hose was run through a plastic cable cover to allow smooth distribution of resin without leaving a hose-shaped indentation in the laminate. The vacuum was connected to the perimeter hose while the resin was fed through the center hose. A resin trap was used to avoid sucking resin from the layup into the lab's vacuum system (Figure 7). Due to the size of the layup, the plastic bag utilized two separate sheets of plastic connected by plumbing sealing putty. The vacuum seal was tested by clamping the resin input hose and visually and aurally inspecting the bag. Leaks were usually in the sealing putty, so they were fixed by either reforming nearby putty or adding more to plug the hole. Once the bag was confirmed to be airtight, the resin was prepared by mixing the resin component with the hardening component, using approximately twice the recommended volume per surface area to avoid resin deficiencies. The input hose was then submerged in the resin, the vacuum was turned on, and the hose clamp was released, allowing the resin to flow into the system. After the resin container had emptied, the input hose was clamped to ensure the integrity of the vacuum. The sample was then left overnight under vacuum to cure. This technique produced a flat laminate with evenly distributed resin and a 0°/90°/+45°/-45° fiber alignment. After separating the laminate from the steel plate and the non-stick cloth, it was left for at least three days to completely dry.

Biofoam

The polyurethane foam was produced by the Chemical Engineering department using various green materials including castor oil and spent rice hulls. The full process

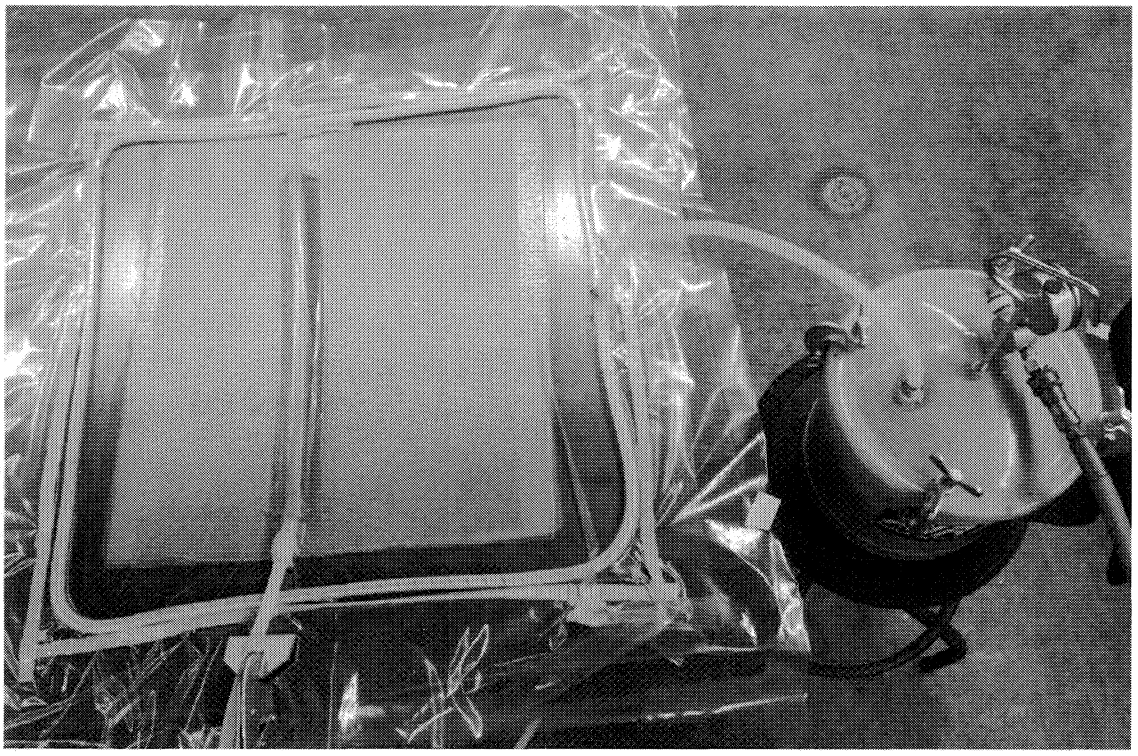

FIGURE 7: Final setup of the vacuum infusion process, after resin has been added. Shows the resin trap (right) and input hose clamp (bottom left).

including the chemistry behind it is described by Mendez et al. (Mendez et al. 2013). What follows is a brief summary.

As described in the literature, creating polyurethane foam requires a polyol, isocyanate, catalyst, foaming agent, and surfactant. The polyol used here was created using castor oil as a base, rather than the usual petroleum based oil. Diphenylmethane 4,4'-diisocynate (MDI), dibutyltin dilaurate (DBTL), water, and silicone oil were the isocyanate, catalyst, foaming agent, and surfactant, respectively. The polyol, DBTL, water, and silicone oil were combined and mixed in one beaker, while the MDI was melted in a separate container. The polyol mixture and the MDI were combined and stirred in a plastic cup for one minute, then allowed to foam.

As reinforcement for some of the foam samples, waste rice hulls were added during the mixing process. Some of these rice hulls were cooked in a furnace at 750°C until the organic material had completely burned off, leaving a white silica ash (Figure 8). Other rice hulls were simply washed with a diluted hydrochloric acid solution to clean off any contaminants or residue. Varying combinations of the cooked and uncooked rice hulls were added when the MDI was added to the polyol mixture. Five different weight ratios of added rice hulls were tested. For cooked rice hulls, weight ratios of 3% and 5% were tested. For uncooked rice hulls as well, weight ratios of 3% and 5% were tested. Each of the foams was given one week to cure before material testing was performed.

Sandwich Biocomposite

The sandwich biocomposite was fabricated according to the specifications in the American Society for Testing and Materials (ASTM) standard D7250-06

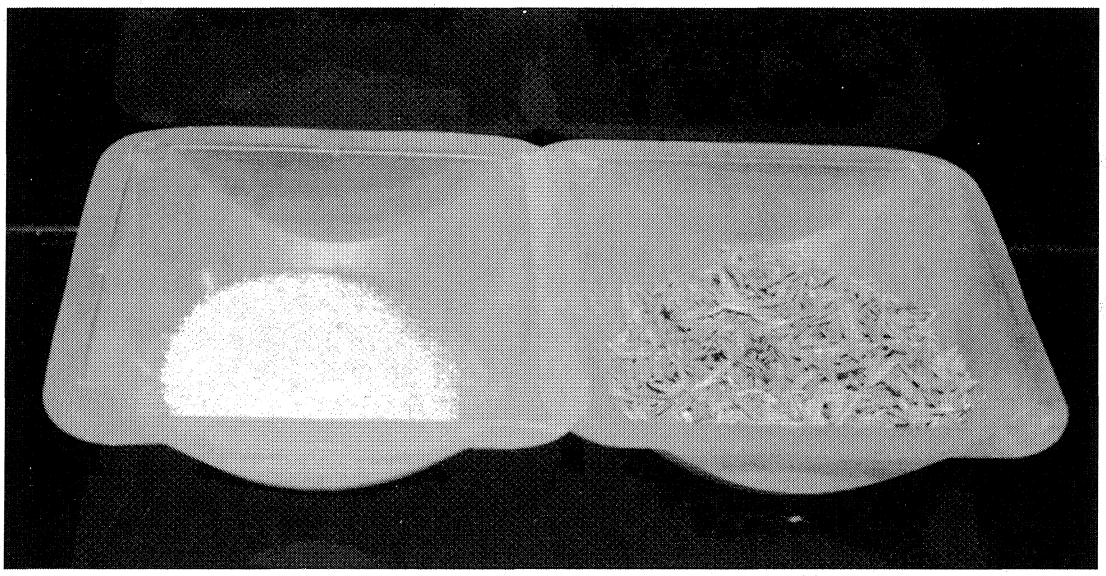

FIGURE 8: Waste rice hulls (right) and the silica ash resulting from the cooking process (left). Picture taken by Lisa AungYong.

(ASTM International 2012a). To comply with the geometry requirements, the final beam dimensions were 7.5" long, 2" wide, and 1" thick (Figure 9). The sandwich thickness consisted of two layers of hemp laminate and one layer of biofoam. Each hemp laminate was 0.06" thick, so the foam was cut into a 0.88" thick rectangular beam. A large rectangular dish was used as the foam mixing container, and a special jigsaw rig was used to ensure a clean, straight cut of the material (Figure 10, Figure 11). A straight cut of the foam is very important because it ensures a consistent surface for the hemp laminate to bond to. The effectiveness of the laminate-foam bond was tested using foam scraps prior to assembling the full sandwich.

Once the components were cut to size, they were glued together using the SuperSap adhesive. To ensure a symmetric composite cross-section, the hemp laminate was attached with the 0°/90° side facing outward on both sides. This symmetric cross-section helps avoid eccentric bending stresses during loading, and keeping the 0° fibers on the outer layer of the composite maximizes the flexural strength by letting the

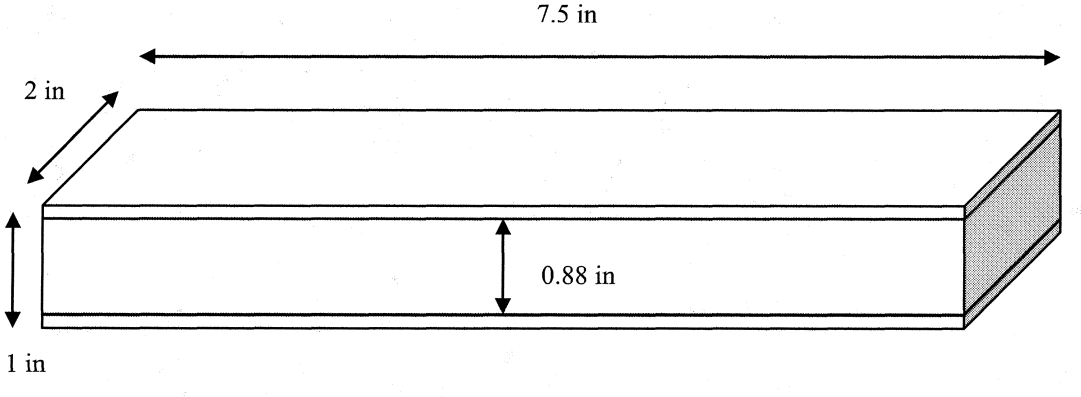

FIGURE 9: Sandwich beam dimensions.

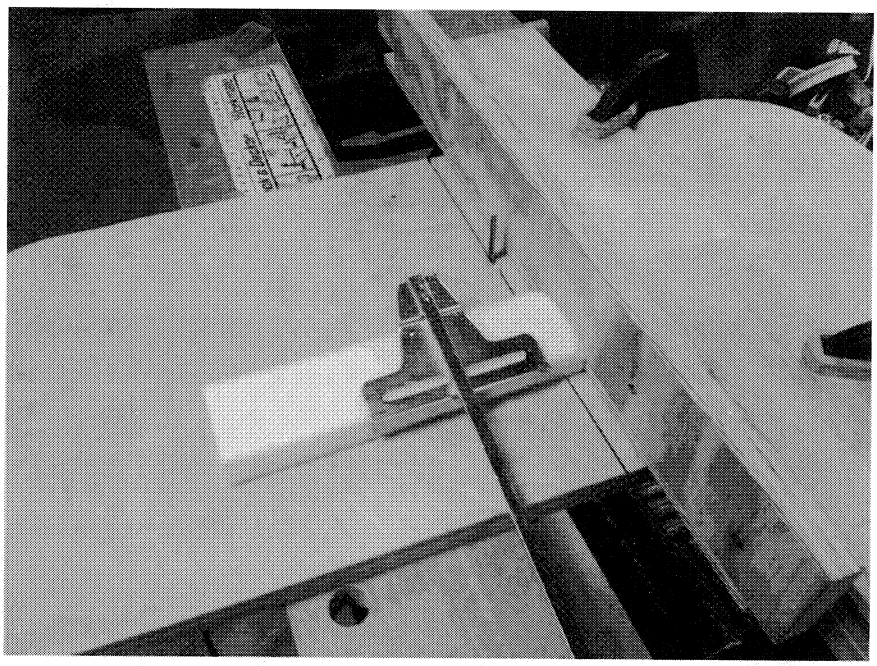

FIGURE 10: Foam cutting setup showing the push stick and guide rail.

FIGURE 11: Underside view of the foam cutter showing how the jigsaw is mounted.

strongest fibers take the greatest load. The sandwich was then left for 3 days to allow the adhesive to set.

Testing

Biofoam

The foam properties were obtained via uniaxial compression tests roughly following ASTM D3575-08 (ASTM International 2008a), and were conducted on a Tinius-Olsen Super L Universal Testing Machine. This test provides the compressive Young's modulus of the foam as well as the plastic yield curve. Although hydrostatic compression and tension tests would be ideal for Abaqus material data requirements, the equipment for such tests is difficult to come by, and was not available for use. The foam samples were either cylindrical or rectangular in shape depending on the production method. The testing machine also utilized a swivel plate attachment to ensure consistent contact with the foam surface (Figure 12).

Because the foam is highly compressible, with no clear ultimate failure point, the test was set to stop after a displacement equal to 75% of the sample height (75% engineering strain). This ensured that the output included all three stages of foam compression (elastic, plastic yielding, and densification). The test was run at 0.25 in/min to allow a complete test within a reasonable time limit. The program gave an output of force and position, which were used to calculate the stress and strain of the sample.

Two sets of compression tests were run. The first set of tests was used to determine the optimal use of waste rice hulls as foam reinforcement. This was accomplished by testing 5 samples with varying amounts of either cooked or uncooked rice hulls. These samples were made separate from each other in round plastic cups, and

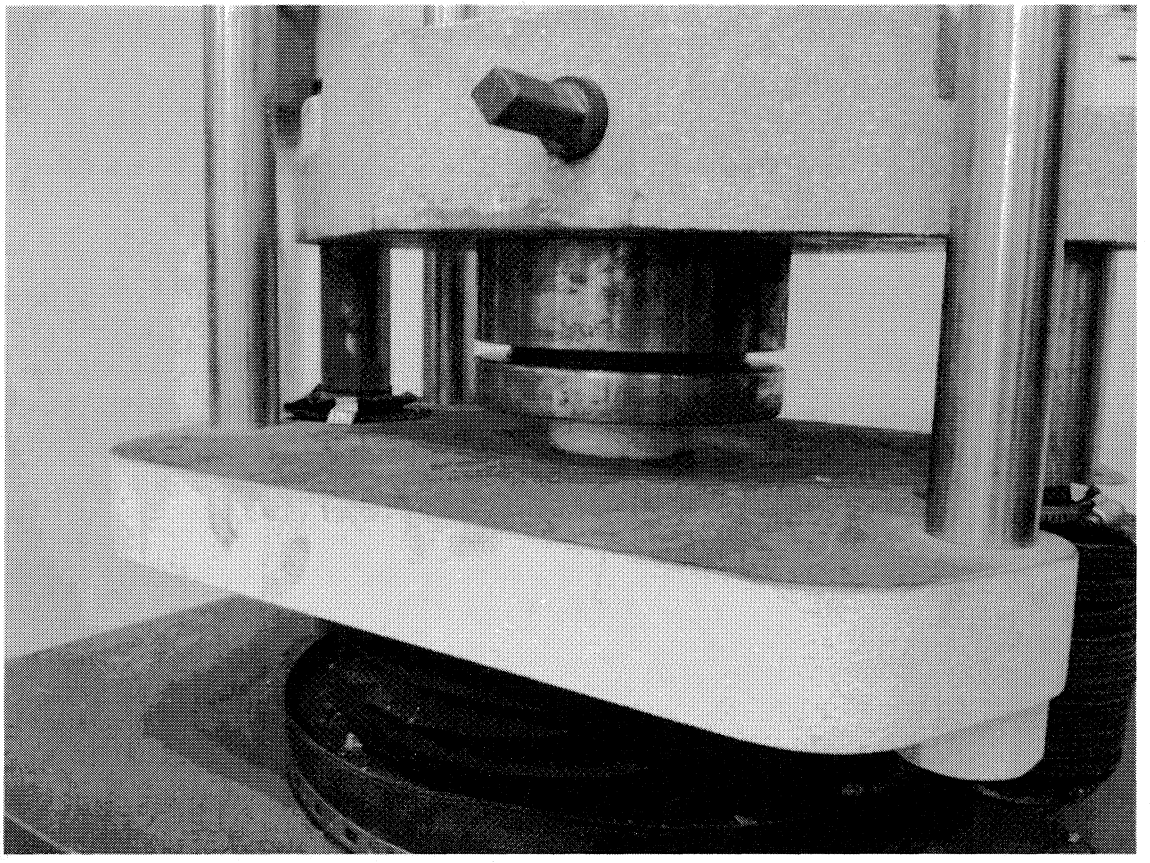

FIGURE 12: Overall testing setup for the foam compression test. Note the swivel plate attachment on the upper loading block.

were therefore 3 inches in diameter and about 1.25 inches in height (Figure 13). Minor height variations were accounted for during the testing and analysis. One sample was pure foam, with no rice hulls added. The remaining 4 samples used either the cooked or uncooked rice hulls, mixed in either 3% or 5% weight ratios. As there was only one sample of each individual foam type, the test results were used to determine a trend relating the use of waste rice hulls with the foam's overall compressive strength.

Following the analysis of the first set of tests, several more samples of the strongest foam were fabricated to obtain more precise material response data for use in

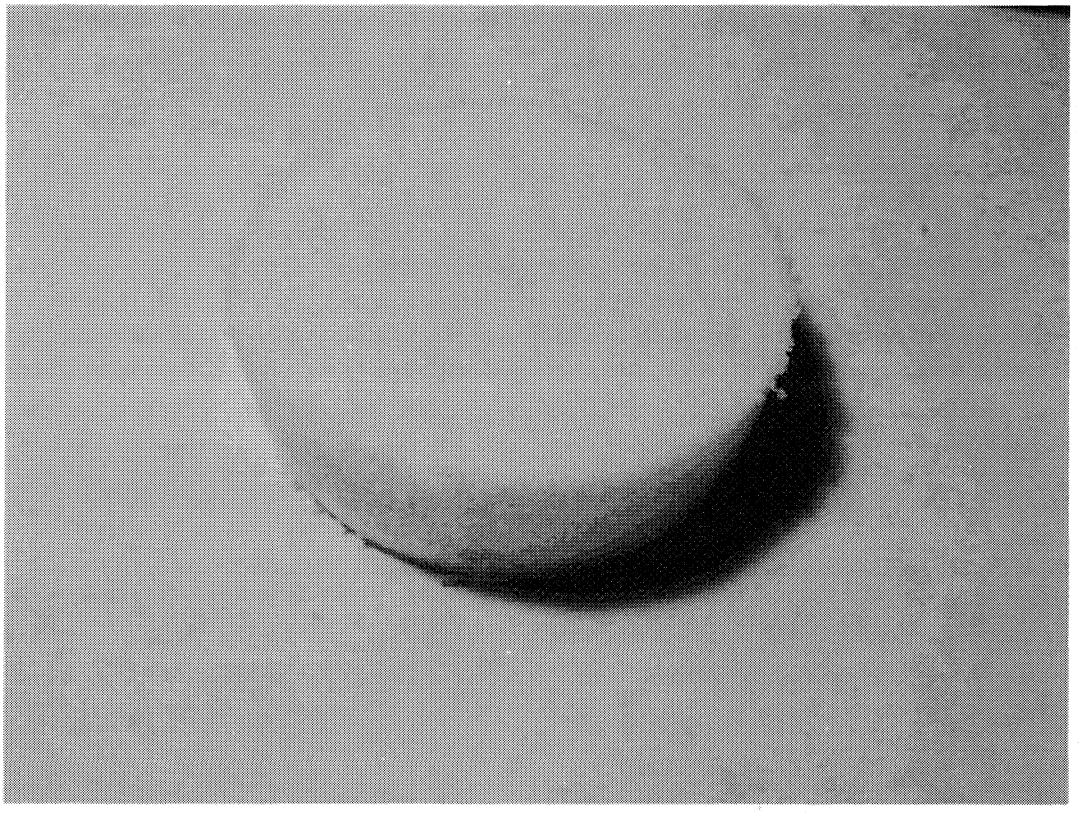

FIGURE 13: Cylindrical foam for compression test.

the numerical model. To ensure consistency with the foam used in the final sandwich specimens, one of the sandwich foam beams was cut into four rectangular pieces for this compression test (Figure 14). These four pieces were then tested using the same methods as the previous compression tests. According to ASTM 3575-08, 4 samples are sufficient to establish statistical significance of the test results if the results sufficiently agree with each other.

Hemp Laminate

The hemp laminate was tested in uniaxial tension according to ASTM D3039 (ASTM International 2008b). This testing mode provides the tensile elastic modulus, yield stress/strain, failure stress/strain, and Poisson's ratio. Compressive tests were not

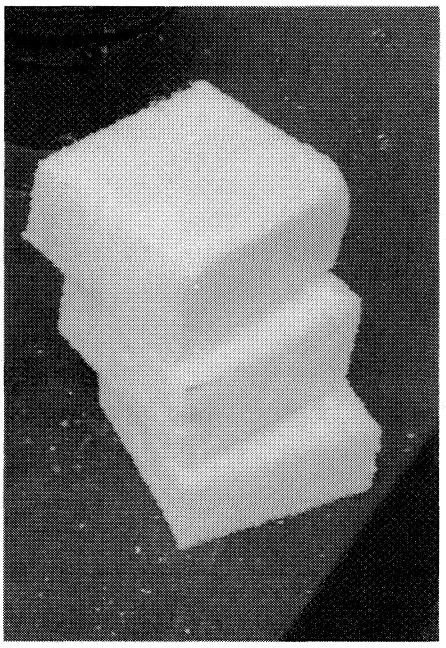

FIGURE 14: Cut up sandwich foam for compression tests.

performed due to the thin nature of the laminate. Any compressive tests normal to the laminate plane would find the material nearly incompressible, while a test parallel to the laminate would likely fail in buckling, which is a complex failure mode that was not anticipated in this problem. The tensile results were assumed to apply to the material in both compression and tension.

In accordance with ASTM D3039, the hemp plates were cut into 3/4" x 24" rectangular coupons. They were cut much longer than the intended gauge length of 10"-15" so that additional gripping clamps could be added to the extending material for slip prevention (Figure 16). For statistical significance, 6 separate plates were tested. Each plate had two biaxial strain gauges attached to each side in the plate center (Figure 17). Two gauges were necessary due to the asymmetrical layout of the laminate (0°/90°/+45°/-45°), which could potentially cause bending during the test. These strain

gauges were used to determine the Poisson's ratio of the material as well as recording the local strain in the material. The readings from each side were averaged to determine these material properties. The test was run at a rate of 0.01 in/min until failure.

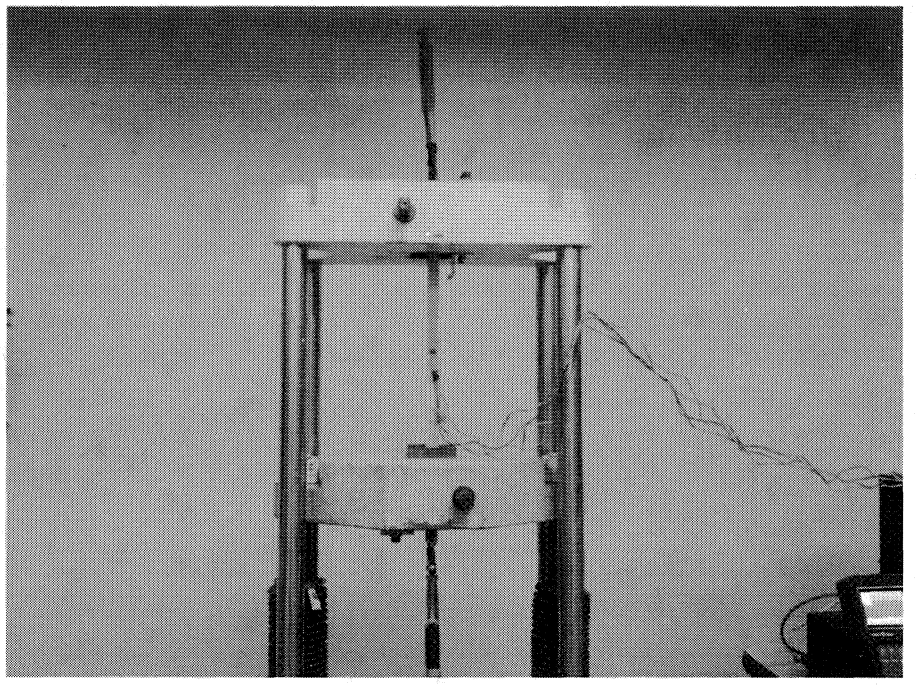

FIGURE 15: Overall setup for the uniaxial tensile test.

Sandwich Biocomposite

As the focus of this study was on the flexural capabilities of the novel material, the sandwich composite was tested in 3-point-bending according to ASTM D 7250-06 (ASTM International 2012a). This test assesses the flexural capabilities of the material without the potential interference of other failure modes such as crushing or buckling. Longitudinal compression and tension tests were not considered because the sandwich material's intended purpose was for non-structural panels in building design, which

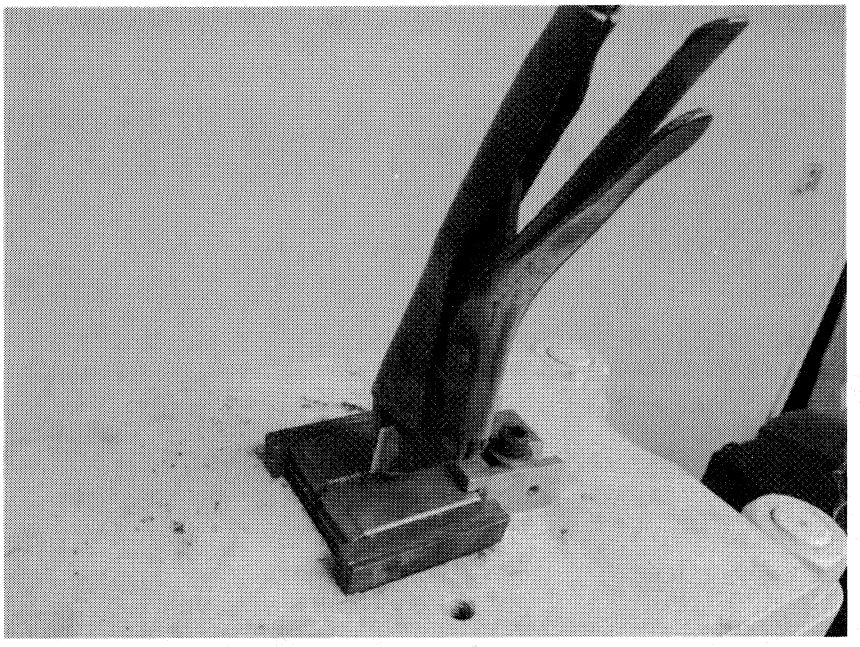

FIGURE 16: Close-up view of the additional clamps used to restrain the hemp plates during the uniaxial tensile test.

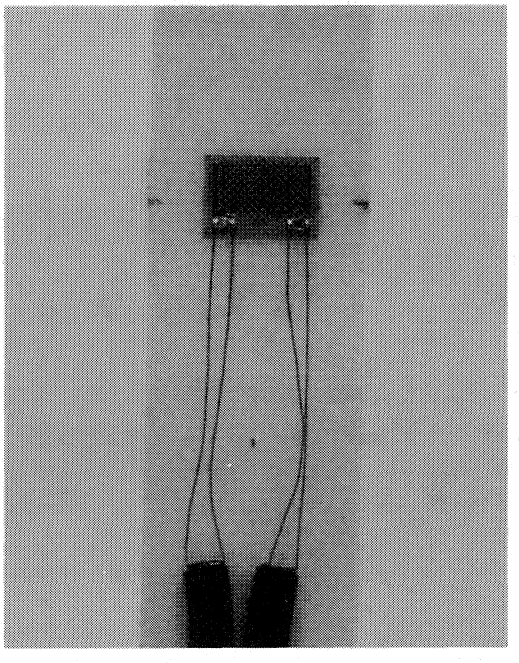

FIGURE 17: Close-up view of the biaxial strain gauge.

support only normal flexural loads, not longitudinal loads. As detailed in the Materials section, the test coupon was cut according to ASTM specifications (Figure 9). The testing machine was outfitted with a 3-point-bending attachment with the supporting rollers adjusted to be 5.5" apart and the single loading roller in the center (Figure 18). The testing coupon was then centered on the apparatus and the test was run at a displacement rate of 0.5 in/min until failure. A grid was drawn on the side of the sandwich to help visualize any deformation within the foam.

Finite Element Modeling

Testing Geometry

The sandwich beam was modeled using the finite element software Abaqus/CAE. This program allows for nonlinear analysis and has many options for modeling material properties, and is therefore well suited for this study.

The laminate face sheets were modeled as planar composites, with an assigned thickness of 0.06 inches. Following the assumption of orthotropy, the planar element was deemed appropriate for this case. Additionally, the planar elements allowed the use of the Hashin laminar failure criterion for modeling damage. Due to the symmetric fiber arrangement, the same failure stresses were applied to both the fiber and transverse directions in the Hashin failure material input field. These failure stresses were obtained from the laminate tension tests.

The foam was modeled as isotropic, with elastic-plastic behavior. The elastic behavior was modeled with the basic Elastic material model. The plastic behavior was modeled with the Crushable Foam material model using the Volumetric Hardening option. This option included Hydrostatic Yield Stress Ratio, a value relating the

FIGURE 18: 3 point bending setup.

foam's strength in hydrostatic tension vs. hydrostatic compression (Dassault Systèmes 2010). As no hydrostatic testing equipment was available for this study, this value had to be estimated through experimentation. The default value was 0.1, but as mentioned in the literature, this assumption is generally inaccurate. Experimentation with different ranges for this value found that it actually had a significant effect on this test, due to the shear forces experienced by the foam core. A value of 0.5 was chosen to accurately model the material.

Although the foam experienced great elastic recovery, this recovery was highly rate-dependent, so for the purpose of this model the foam was considered perfectly plastic. Failure data for the Crushable Foam material model was derived from the foam

compression tests. Due to the sensitivity of the equipment, the raw data from the compression tests showed moderate fluctuations at low strains. Because the program does not accept decreasing stress values for material property definitions, an open source digitizing software called Plot Digitizer was used to generate a separate, smoother curve that matched the raw data as closely as possible (Figure 19).

The foam and hemp parts were connected with surface to surface ties, creating a perfect bond. This followed the assumption that the bonding adhesive was much stronger than the foam, so any delamination would occur within the foam material itself rather than at the point of bonding.

Analytical rigid surfaces were used to simulate the rollers from the experimental test. Each surface was a semicircle with a radius of 0.5" and extended the full width of the beam. The interaction properties between the rollers and the beam surfaces were set to hard contact with a coefficient of friction equal to 0.001. This small coefficient of friction was used in preference to the frictionless property in order to avoid convergence issues caused by frictionless surfaces.

The model mesh was designed to achieve satisfactory convergence with a sufficiently fine mesh while still being able to complete the simulation within a reasonable time frame. Due to the expected locations of stress concentrations around the loading and support rollers, the parts were partitioned to allow localized mesh refinement in those areas. Additionally, the fine mesh at these locations prevented excessive penetration between the roller surfaces and the beam. The figures below show the partitions and an example of a locally refined mesh (Figure 20 & Figure 21).

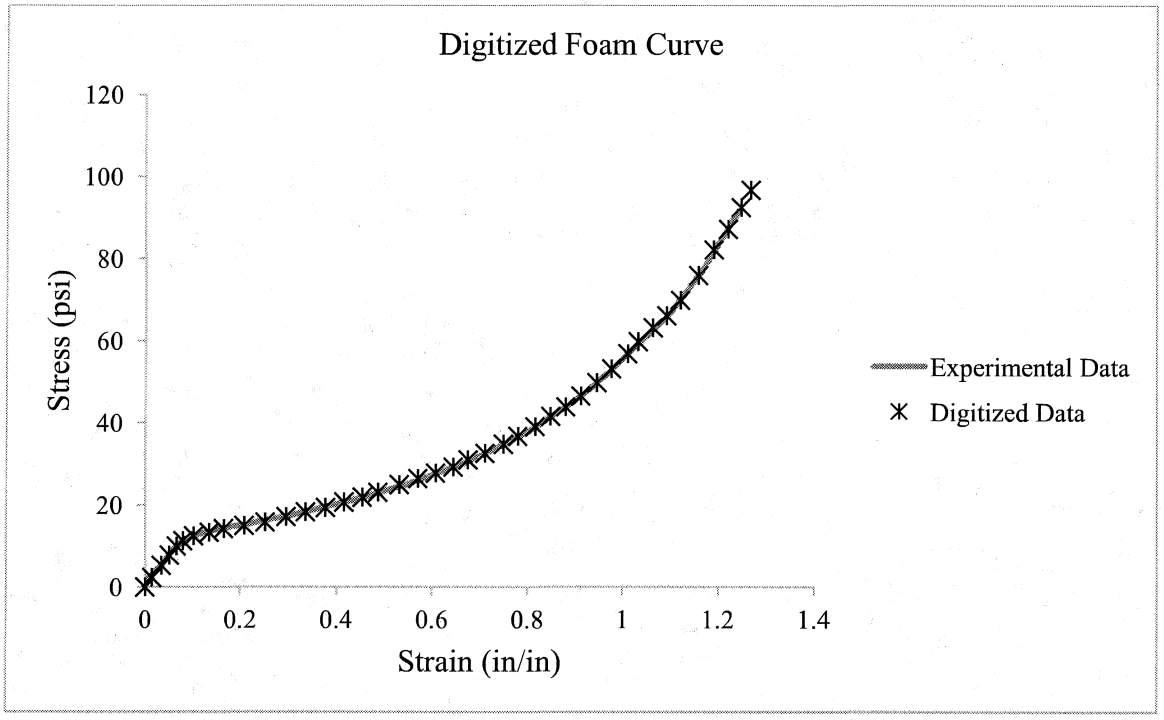

FIGURE 19: Digitized stress-strain curve for the 5% cooked foam.

The job was run as a static, Riks analysis with nonlinear geometry enabled. The Riks method was designed for buckling and other problems with large deformations, making it suitable for this simulation. Due to the potentially complicated nonlinear

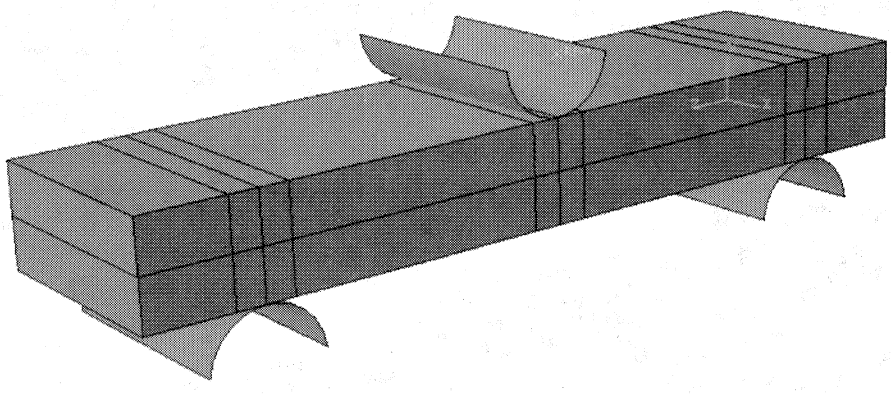

FIGURE 20: FEM Sandwich partitions for localized mesh refinement.

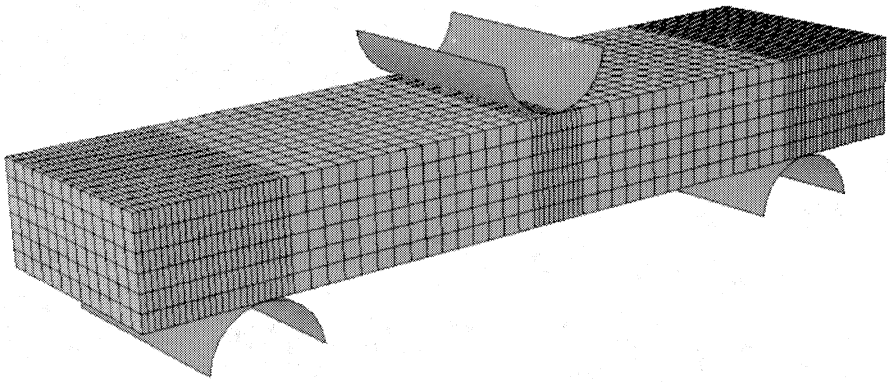

FIGURE 21: Example of localized mesh refinement following the above partitions.

response, the convergence allowances for both minimum time increment and maximum number of steps were increased substantially from their default values.

Drywall Comparison

Once the model was validated, the same materials and interaction properties were applied to alternate beam geometries in order to compare them with existing requirements for other non-structural building panels. In particular, they were compared to gypsum wallboard, one of the most common types of interior wall panels. The standard flexural test for gypsum wallboard is described in ASTM C473-12 (ASTM International 2012b). For consistency with the other tests in this study, Method B was used to simulate a constant cross head speed. In this test, the specimen is cut into a 12 in by 16 in rectangle, and placed into a 3 point bending setup with supports spaced 14 inches on centers. The load and supports are applied by rollers with a radius of 0.125 in. The specimen strength is recorded at the breaking point of the gypsum board, and must exceed the minimum specifications given in Table 1.

To directly compare the sandwich board to drywall, the finite element model used the same material and interaction properties that were previously validated and applied them to the geometry listed in ASTM C473-12 (Figure 22). Because most of the parameters were set by the test, the only variables that were inspected were the overall sandwich thickness and the number of face sheet layers on the top and bottom of the board. Additionally, because the sandwich material often does not break in brittle failure, the maximum load experienced by the model was used for comparison to standard drywall strengths.

As part of this test, ASTM also recommends testing orthogonal cuts of the drywall. This is due to the way drywall is produced, which introduces an inherent anisotropy where the board is stronger along one axis than on the other. However, the sandwich beam studied here was constructed to be orthogonally symmetric, and this symmetry was assumed in the finite element model. Thus, only a single rotational configuration was considered for the sandwich material. Minimum strength requirements

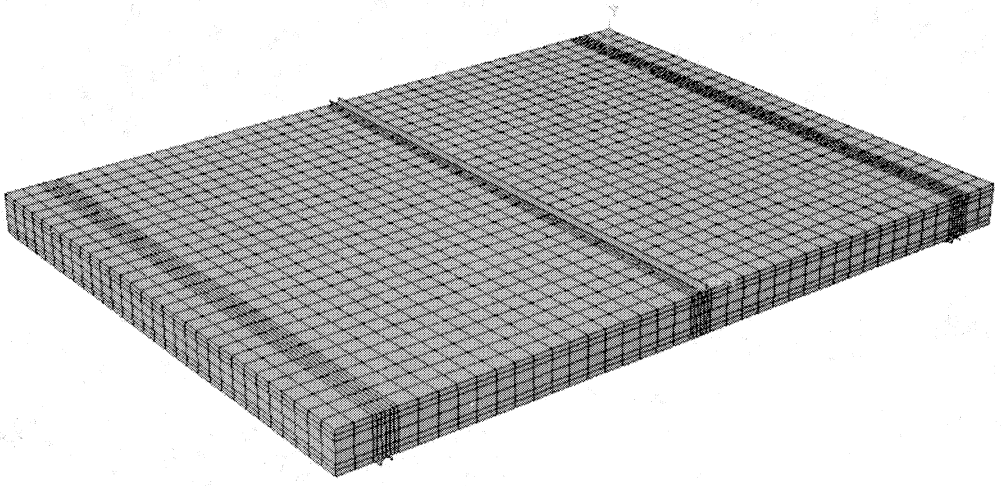

FIGURE 22: 1" thick sandwich panel for drywall comparison.

for gypsum wallboard are listed in ASTM C1396-13 (ASTM International 2013), with the flexural requirements summarized in Table 1. These values were compared to finite element results for varying sandwich geometries to determine the potential for replacing gypsum wallboards of various thicknesses.

TABLE 1: Minimum Flexural Properties of Gypsum Wallboard (ASTM International 2013)

Board Thickness (in.)	Strong Axis Failure Point (lbs.)	Weak Axis Failure Point (lbs.)
1/4	46	16
5/16	62	21
3/8	77	26
1/2	107	36
5/8	147	46
3/4	167	56

Assumptions and Limitations

Due to restrictions on time, materials, and available testing apparatus, some simplifying assumptions were made in these tests. These assumptions are listed below.

Both the compressive and tensile behaviors of polymeric foams are temperature dependent (Zhang et al. 1997). Increased temperatures lead to a significant decrease in foam stiffness, strength, and energy absorption capacity. However, the tests presented here assume all the materials to be at a constant room temperature. It was expected that this temperature should be relatively consistent with ambient temperatures in the average household where these panels are proposed for use. If significant temperature

fluctuations are expected during the lifetime of this material, then further tests regarding temperature dependence are recommended.

ASTM 3039-08 (ASTM International 2008b) recommends a symmetric layup for the fiber-reinforced polymer test coupon. Unfortunately, while the final sandwich layup was designed to be perfectly symmetric (0°/90°/+45°/-45°/Foam/-45°/+45°/90°/0°), the individual hemp laminate plates were actually asymmetric (0°/90°/+45°/-45°). Such asymmetric layups are generally avoided because the difference in stiffness between each face can cause bending in the plate. Due to constraints on the thickness of the beam, however using 4 layers of woven hemp fabric to make the laminate was deemed unfeasible. Therefore, bending was very likely during the uniaxial tensile tests, and the strain gauge readings on either side of the laminate were averaged to obtain the overall Poisson's ratio.

Another common result of an asymmetric layup is that orthogonal cuts from the same material will behave differently due to the interaction between the coupon bending and the outer fiber alignment. This is generally the case with unidirectional fiber layers. In this case, however, the fibers were woven together, so the 0°/90° fiber layers actually existed in the exact same plane. Therefore, a sheet of woven fabric should be perfectly symmetric about a 90° rotation, and the laminate resulting from these sheets should share the same symmetric properties. Given sufficient time, this assumption would be tested by comparing the tensile strengths of orthogonally cut coupons. However, there was insufficient time for these verification tests, so orthogonal symmetry was assumed in the composite laminate.

These tests assume the tensile and compressive moduli to be identical for both materials. While this assumption might not necessarily hold true, the measured properties were obtained in the most prominent load conditions for each individual material. Thus, any resulting errors should be fairly minor.

Additional requirements and tests for gypsum wallboard include fire resistance, water absorption, nail pull resistance, and thermal conductivity. However, this study focuses only on the structural strength of the material. Further studies are required to fully validate this novel biocomposite as a replacement for gypsum wallboard in non-structural building applications.

CHAPTER 5

RESULTS

Foam and Laminate Material Testing

While the testing program was capable of calculating stress and strain on its own, only the raw data was used in this experiment to avoid any unseen errors. This raw data consisted of force from the load cell (F_{lc}) and the displacement of the crosshead (u). These values were converted into stress and strain using the following equations.

Stress:

$$F_{adj} = F_{lc} - F_0 \tag{6.1}$$

$$\sigma = \frac{F_{adj}}{\left(\frac{D}{2}\right)^2 * \pi} \tag{6.2}$$

Where:

F_{adj} = Adjusted force (lbs)

F_{lc} = Force from load cell (lbs)

F_0 = Initial force from load cell (lbs)

σ = Engineering stress (psi)

D = Diameter of sample (in.)

Due to the sensitivity of the machine, the initial force value was not exactly at zero, and varied between the different material tests. Equation (6.1) ensured that the data began at zero force. Equation (6.2) calculated the engineering stress in the specimen.

Engineering stress differs from true stress in that it does not account for changes in the cross-sectional area of the sample. An example of such change would be necking during ductile tensile failure. However, the testing equipment could not measure the change in radius of the specimen, and such cases were deemed unlikely or insignificant in both material tests. Due to the crushability of the foam, it was assumed that the radius would not change significantly over the course of the test, while the hemp composite was assumed to fail prior to any necking effects taking place. Therefore, the use of engineering stress was deemed valid.

Strain:

$$u_{adj} = u_{lc} - u_r \tag{6.3}$$

$$\varepsilon = \ln\left(1 + \frac{u_{adj}}{h_{sample}}\right) \tag{6.4}$$

Where:

u_{adj} = Adjusted displacement

u_{lc} = Displacement from load cell

u_r = Reference displacement

ε = True strain

h_{sample} = Sample height

As with the force adjustment, equation (6.3) modified the resulting curve to ensure reasonable results. Unlike the force adjustment, however, the strain was adjusted so that the initial elastic region of the stress-strain curve intersected well with the origin. The particular reference displacement was determined empirically. Equation (6.4) calculated the true strain of the material. While engineering strain is simpler to calculate,

it is only accurate at very low strain levels (Figure 23). Due to the very high strains experienced by the foam samples, and the relative ease of large scale computations using Microsoft Excel, this experiment utilized true strain.

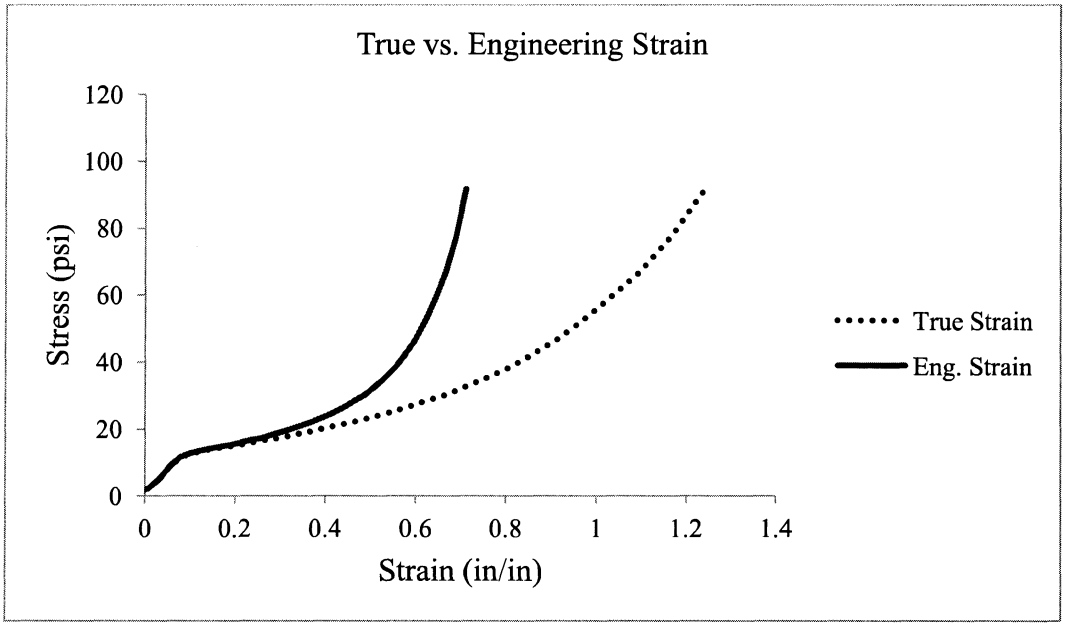

FIGURE 23: Comparison of true strain vs. engineering strain at high compressive strains. For clarity, compressive stresses and strains are displayed as positive.

Foam

The first set of tests compared foams with various weight ratios of waste rice hulls used for reinforcement, and found that the addition of cooked rice hulls resulted in increased foam strength. The pure foam compression test included an unloading section at a strain of roughly 25% to check the foam's short-term elastic recovery (Figure 24). While the resulting curve suggested a fully plastic material, the elastic recovery was found to be highly rate-dependent, as the foam samples returned very close to their original heights after about 5 minutes. However, this study was focused on the relatively

immediate case of flexural loading and failure, so the foam was considered to be an elastic-perfectly plastic material for the purpose of these tests and the following numerical simulations.

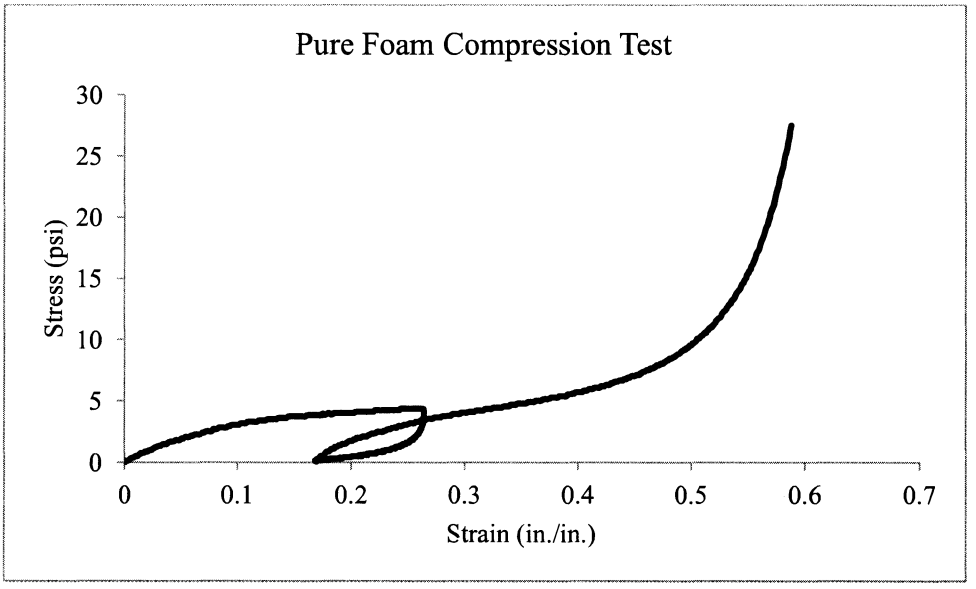

FIGURE 24: Uniaxial compression test results for pure foam sample.

The addition of cooked rice hulls to the foam mixture provided a noticeable increase in strength (Figure 25). Both the Young's modulus and the yielding stress were progressively improved for the 3% cooked and 5% cooked foams, with the 5% cooked curve showing the most distinct increase. This indicates that the silica ash left after burning off the organic material in the rice hulls is capable of bonding with the foam material without compromising the integrity of the foaming reaction. However, the use of uncooked rice hulls exhibited the opposite effect. The foam actually became weaker to the point where it lacked a distinguishable linear elastic region and yield plateau. This

very likely indicates that either the organic material caused an adverse reaction with the foaming chemicals, or the particles were simply too large to properly bond with the foam.

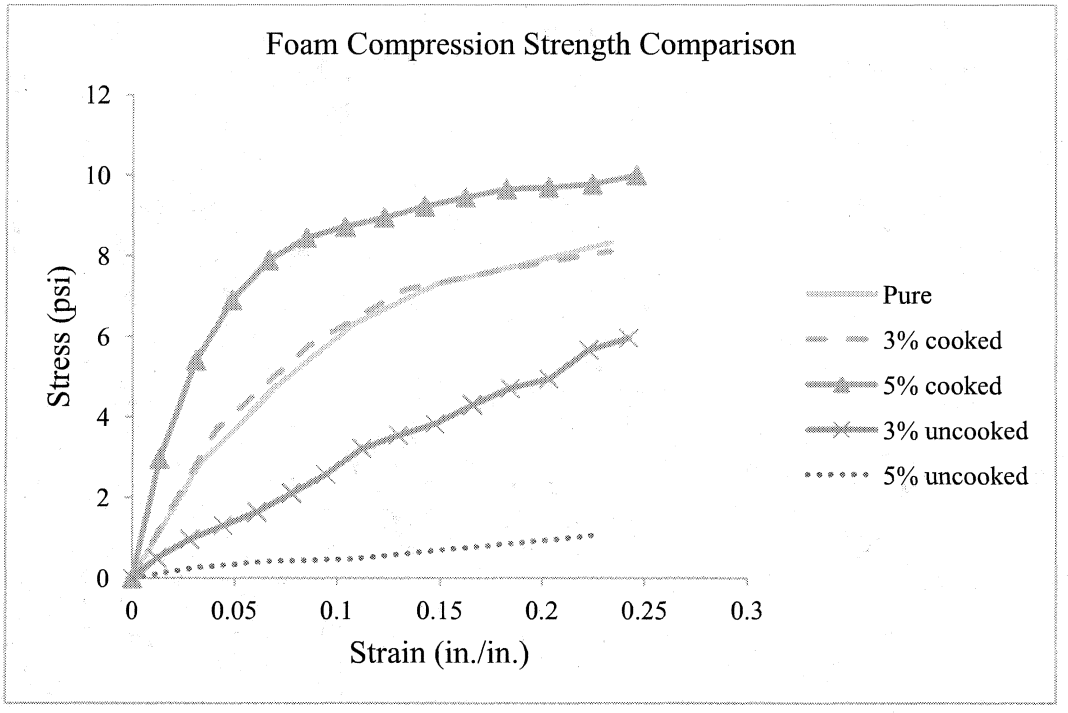

FIGURE 25: Comparison of foam material strength for different amounts of reinforcement with waste rice hulls.

According to these tests, the foam using 5% cooked rice hulls exhibited the greatest strength. Therefore, the remaining compression tests were performed on a cut up sandwich beam using the 5% cooked foam (Figure 14). The results show the linear elastic region lasting until about 0.07 strain, followed by a plastic plateau that smoothly transitions into densification at very high strains (Figure 26). Each of the four samples followed similar trends, but did exhibit some large strength differences. This could be attributed to faults within the tested foam that weakened individual specimens. The

Young's moduli for these four tests are shown in Table 2. There is an unfortunately large variation between the moduli across these four tests. However, due to restraints on time and materials, further testing could not be performed prior to the completion of this study.

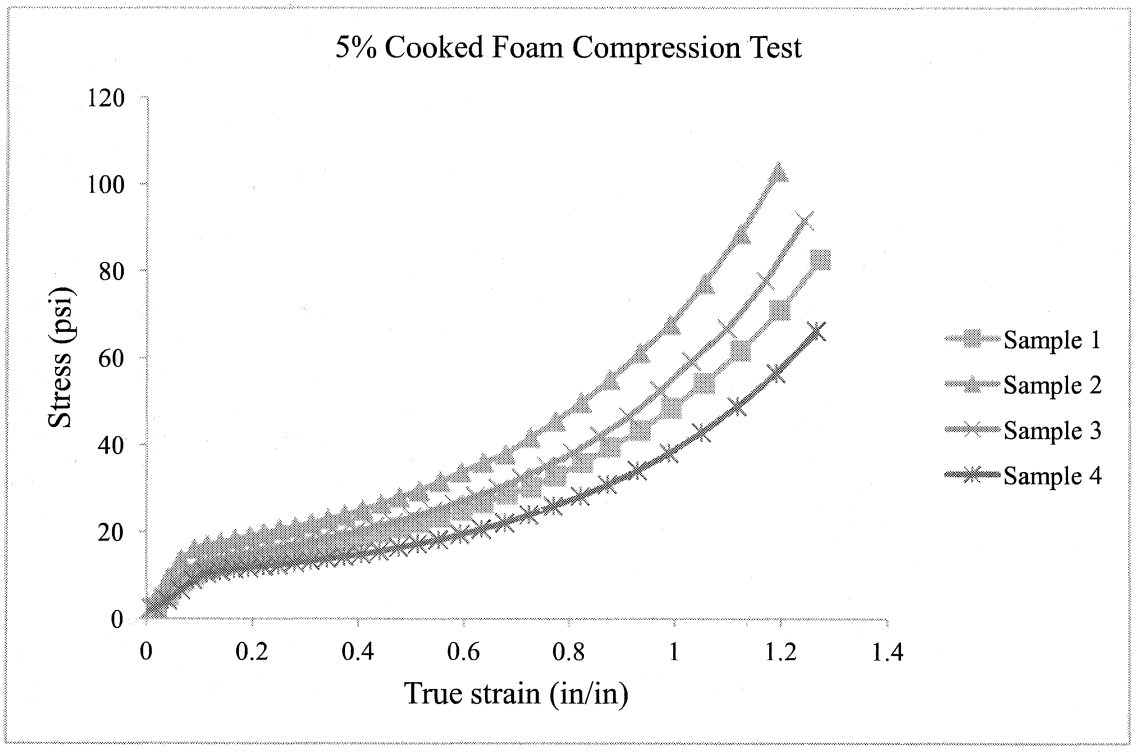

FIGURE 26: Compression test results for 5% cooked foam.

TABLE 2: Young's Modulus Results for Compression Tests of 5% Cooked Foam

Sample/Statistic	Modulus (psi)
1	110
2	140
3	220
4	160
Mean	157.50
Standard Deviation	46.46
Variation	29.50%

Laminate

Results from the uniaxial tensile tests are shown in Figure 27. The results show an initial elastic region up to about 4000-5000 psi, followed by a plastic deformation region where the stress increase begins to slow down as the strain continues to increase steadily. This stress rate decrease follows a steady curve until the stress-strain curve is almost completely horizontal (perfectly plastic). At about 7000 psi, the coupons experienced ultimate failure, illustrated in the figure by a sudden drop in stress. This fits the expected behavior of a fiber reinforced plastic material. The statistical determinations for the material properties are given in Table 3. Because the variation was less than 10% for the Young's modulus and less than 5% for the ultimate stress and Poisson's ratio, the results from these 6 tests could be considered statistically acceptable.

The method for calculating stress and strain was the same as that used in the foam test, using equations (6.1)-(6.4). There was significant initial slip between the loading clamps and the test coupons, so u_{adj} was selected moderately far into the data set to ensure the elastic region of the curve would intersect the origin. As with the foam test, F_{adj} was set to start the loading at zero.

Although great care was taken to ensure even and accurate distribution of pressure from the loading clamps, some bending was observed during loading. This bending was likely caused by the asymmetric layup of the single laminate fibers. Due to this bending, all of the test specimens failed at or near the grip, where the tensile stresses were combined with bending stresses. Therefore, these results most likely underestimate the laminate's strength when integrated into the sandwich composite.

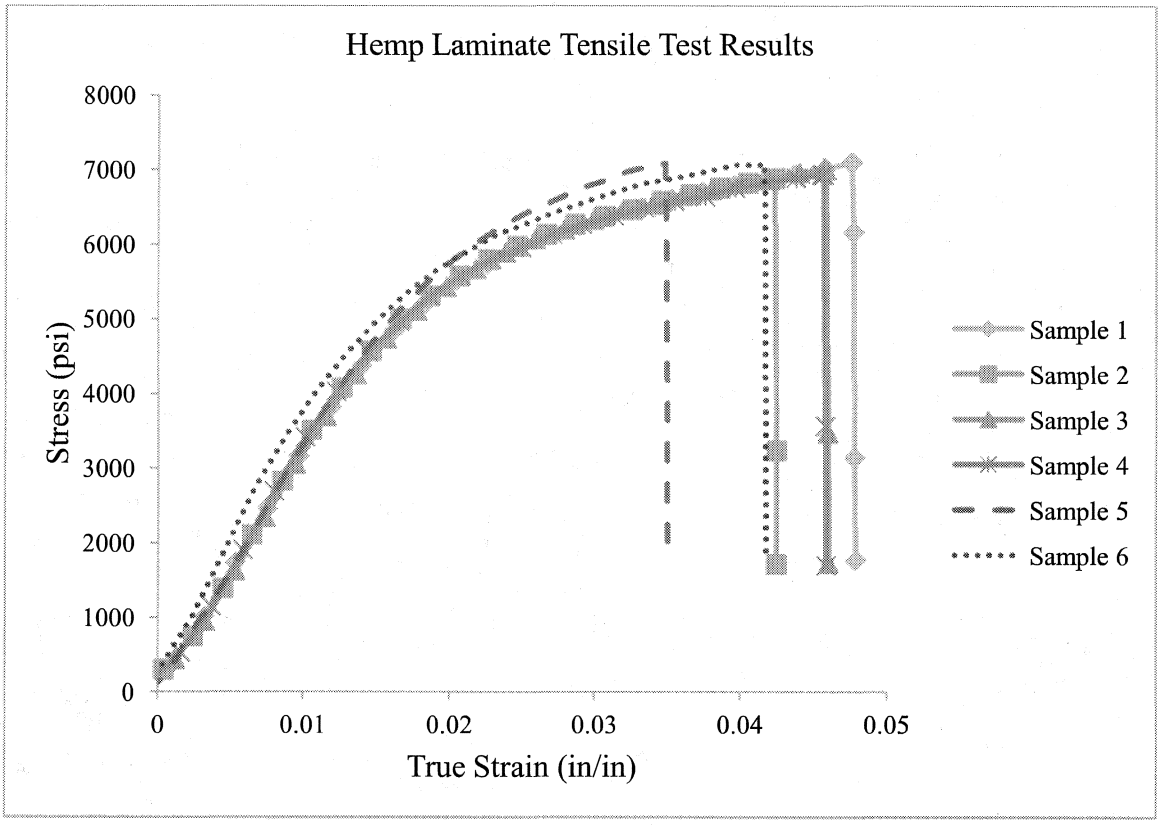

FIGURE 27: Uniaxial tensile test results for hemp composite laminate.

TABLE 3: Material Property Data for Tensile Test of Hemp Composite Laminate

Sample/Statistic	Young's Modulus (psi)	Ultimate Strength (psi)	Poisson's Ratio
1	322000	7080	---
2	325000	6880	0.283979
3	314000	7020	0.266924
4	330000	6930	---
5	339000	7380	0.274867
6	403000	7280	0.255926
Mean	338833.3	7095.0	0.2704
Standard Deviation	32517.2	197.4	0.0119
Variation	9.60%	2.78%	4.41%

3 Point Bending Test

The load-displacement results from the 3 point bending tests are shown in Figure 28. The sandwich experienced a short elastic region as the supported load quickly increased to its maximum at about 1 inch of displacement. Once reaching the peak load, the curve entered a strain softening region where the supported load decreased slightly until about 2.2 inches of displacement. Following this phase, the load dropped at a faster rate before the test completed at 3 inches of displacement.

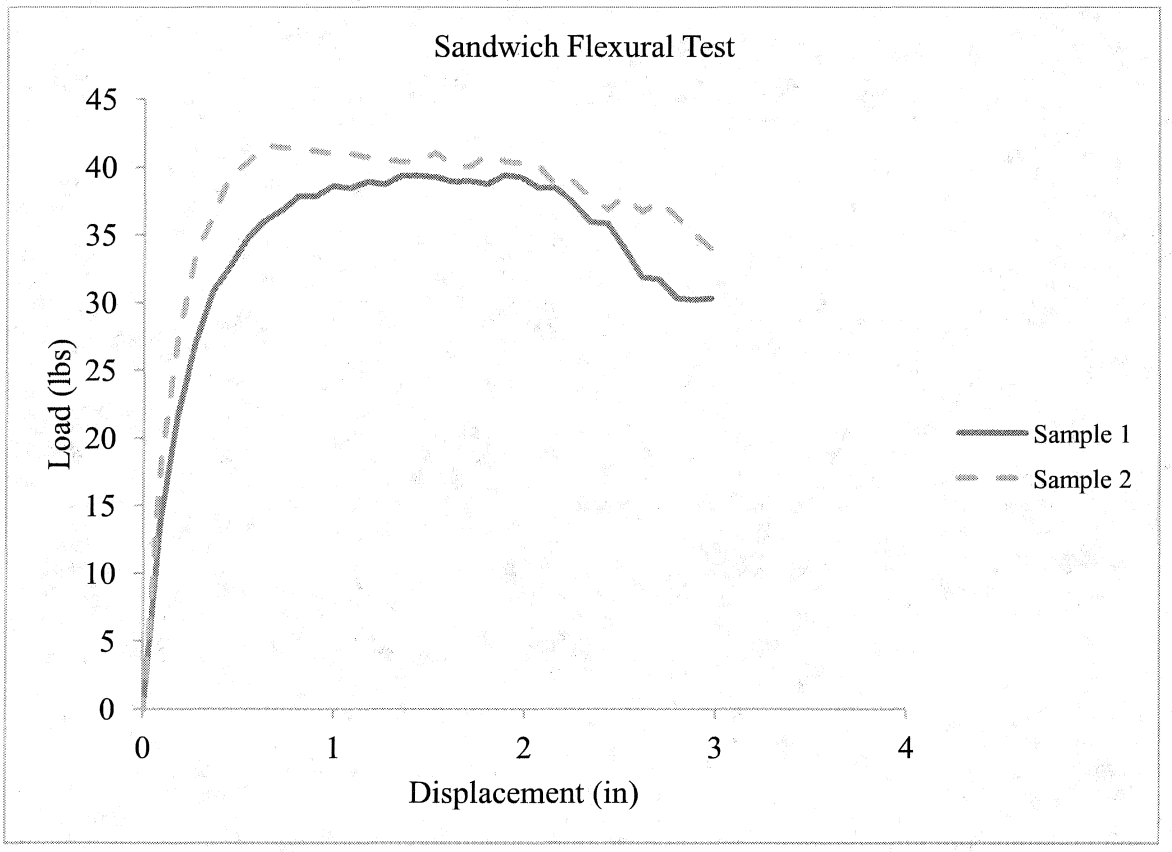

FIGURE 28: Load-displacement results from 3 point bending test of a foam biosandwich.

Although the sandwich did not experience a brittle or catastrophic failure, the initial failure mode was a generalized form of core shear, with the foam core visibly being sheared by the face sheets (Figure 29). This shearing displacement was not enough to cause core shear failure, however. There was also some slight foam compression immediately beneath the loading roller, but this was small enough to still be considered elastic. At greater displacements, this localized compression was much more noticeable, and the core shear effect was even more pronounced (Figure 30). Near the end of the test, the upper face formed a rigid hinge that caused the sandwich center to lose contact with the loading roller (Figure 31). Unloading the beam demonstrated large elastic recovery (Figure 32), but there was moderate damage to the laminate face sheets. In particular, the upper laminate had an easily visible crack in the center of the beam (Figure 33).

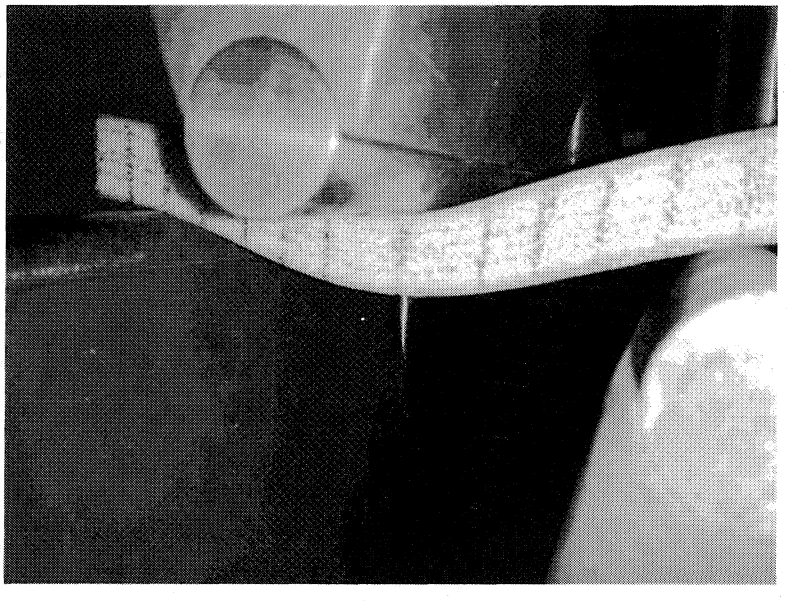

FIGURE 29: Early core shear during 3 point bending test. Note that the vertical gridlines are no longer perpendicular to the face sheets.

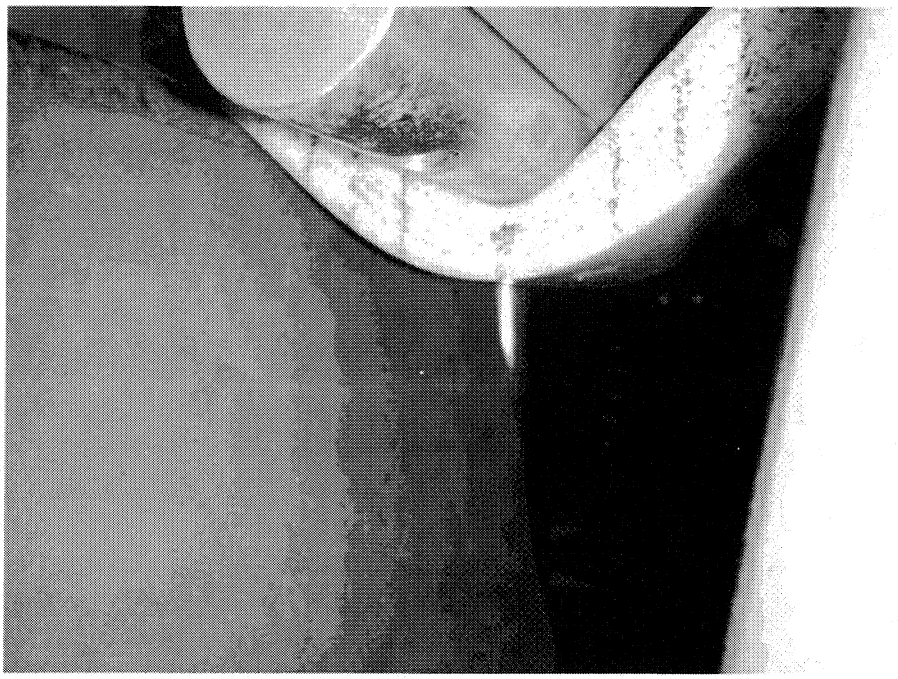

FIGURE 30: Core shear with localized compression during 3 point bending test.

FIGURE 31: Final state of the sandwich 3 point bending test. Note the rigid fold in the top face causing the center to visibly separate from the loading roller.

FIGURE 32: Sandwich condition after unloading. There was significant elastic recovery at this point.

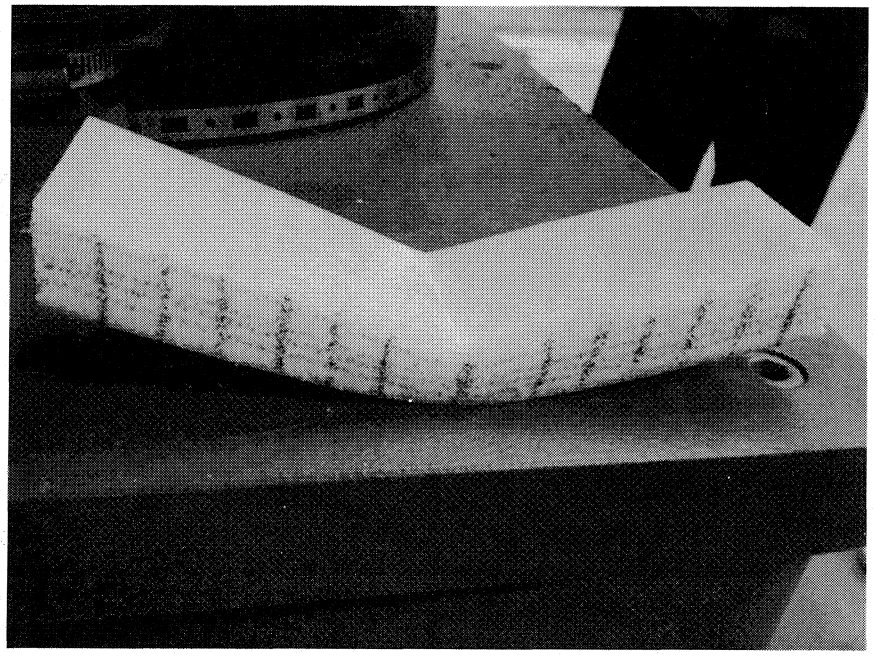

FIGURE 33: Failed sandwich showing the crack in the upper laminate face sheet.

Both sandwich samples followed this failure trend, although sample 2 was initially stronger. This may be due to an imperfection in the sample that required additional resin to completely glue the upper face sheet to the foam. The additional resin may have augmented the initial strength by effectively increasing the upper face thickness. Because sample 2 had a visible imperfection that apparently affected the results, sample 1 was used as a reference for the finite element model.

Finite Element Analysis

Experimental Validation

Load-displacement results from the finite element model are shown in Figure 34. While the original simulation using the average foam strength values showed an overall lower load response compared to the experimental results, an alternate model using the strongest foam strength values agreed very well with the experimental results of sandwich 1. This appears to support the earlier observation that imperfections in the other foam samples led to reduced strength results. The Abaqus curve ended shortly after attaining its maximum load value due to excess element deformations within the model. Thus, while the model cannot model the full behavior range of the sandwich material, it does give an accurate estimate of its maximum strength. With regards to the failure mechanisms, the model showed a combination of general shearing of the core and localized compression in the beam's center (Figure 35). This agreed well with the experimental results, further validating the finite element model as an appropriate representation of the experimental sandwich composite (Figure 36).

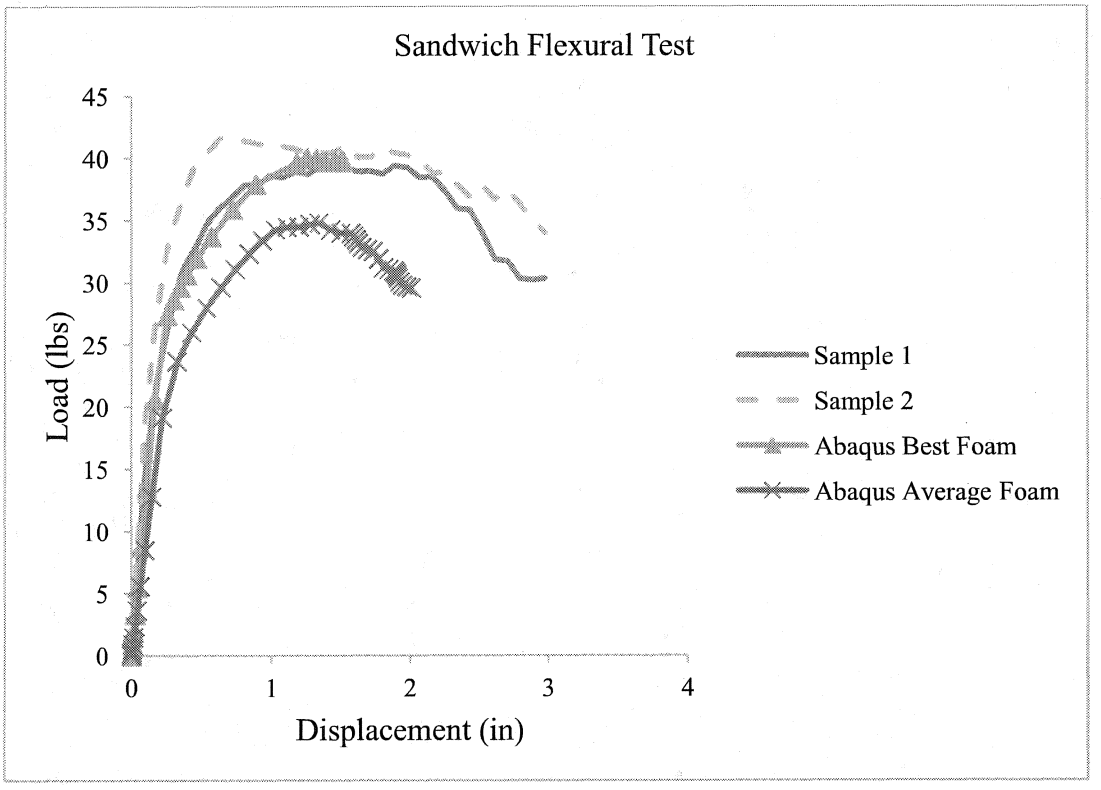

FIGURE 34: Abaqus model output compared to experimental results.

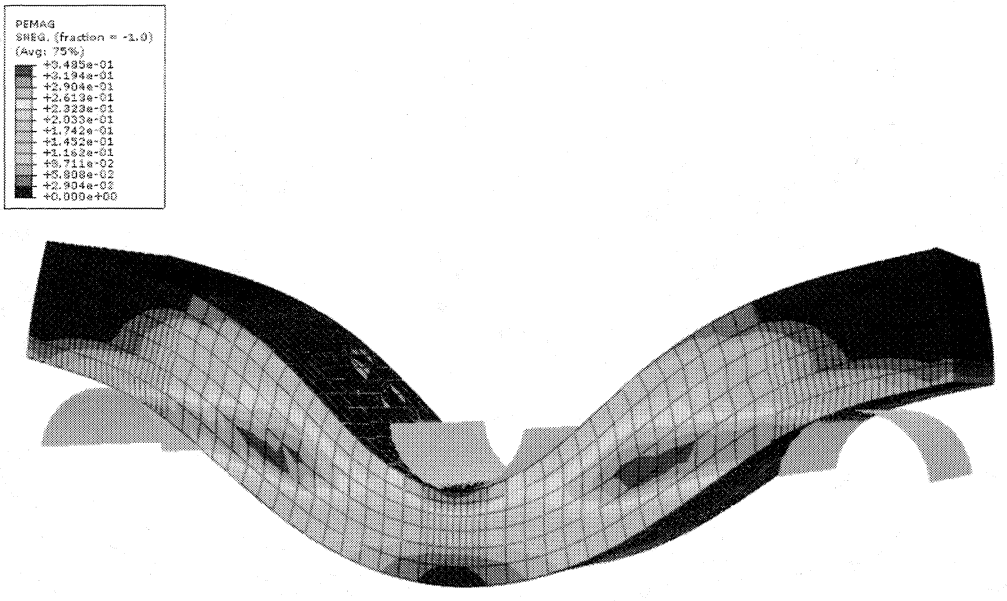

FIGURE 35: FEM output showing the magnitude of plastic strain within the foam.

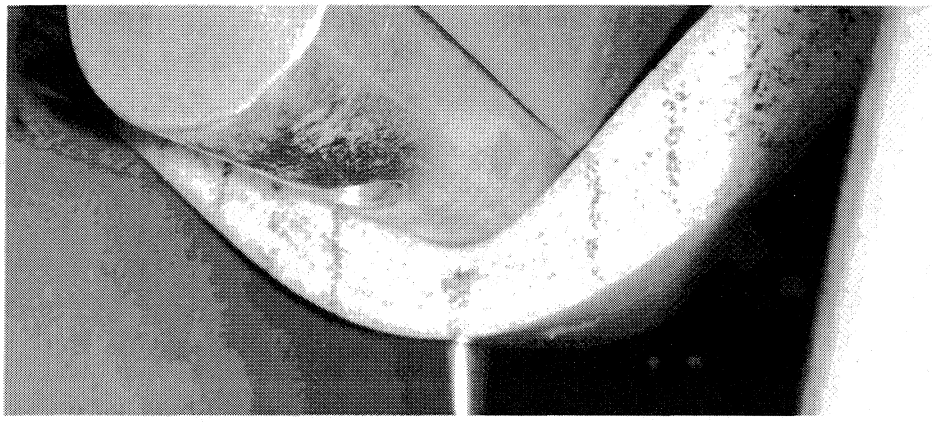

FIGURE 36: Experimental sandwich for comparison showing core shearing and local compression.

Drywall Test Geometry

The agreement of results between the experiment and finite element model indicated that the materials and interactions were modeled with sufficient accuracy to investigate the effects of geometry modifications on the sandwich structure. The inspected variables included foam thickness and number of face sheet layers. Five separate sandwich geometries were simulated: four with single-layered face sheets and overall thicknesses of 1.25, 1, 0.75, and 0.5 inches, and one with double-layered face sheets and an overall thickness of 1 inch.

The maximum strengths of these simulated sandwich panels are summarized in Table 4, as well as a comparison between these strengths and the minimum drywall standards established by ASTM. The values in the table indicate the strength difference between the foam sandwich and the drywall, with positive values indicating a stronger sandwich. In general, the sandwich material is equal in strength to a drywall panel that is

half the sandwich's thickness. This ratio decreases slightly for the 1.25" sandwich, but holds true for the remainder of the tested geometries.

TABLE 4: Foam Sandwich to Drywall Strength Comparison

Sandwich Geometries & Strengths	Drywall Standard Sizes and Strengths					
	1/4" 46 lbs	5/16" 62 lbs	3/8" 77 lbs	1/2" 107 lbs	5/8" 147 lbs	3/4" 167 lbs
1.25" 168.1 lbs	+122.1	+106.1	+91.1	+61.1	+21.1	+1.1
1" double laminate 130.3 lbs	+84.3	+68.3	+53.3	+23.3	-16.7	-36.7
1" 137.5 lbs	+91.5	+75.5	+60.5	+30.5	-9.5	-29.5
.75" 103.4 lbs	+57.4	+41.4	+26.4	-3.6	-43.6	-63.6
.5" 58.2 lbs	+12.2	-3.8	-18.8	-48.8	-88.8	-108.8

The failure modes of the five sandwich geometries are shown in Figure 37 through Figure 41. While three of the five geometries showed ductile failures in either local compression or local indentation, the double layer sandwich and the 0.5" sandwich both showed failures in core shear. Core shear, as mentioned in the literature, is a brittle failure mode, and is undesirable for most applications. It generally occurs when the face sheets are much stronger than the core, which is consistent with the two geometries mentioned here. Thus, sandwich thicknesses smaller than 0.75" are not recommended, nor are double layer face sheets unless much stronger foam is used.

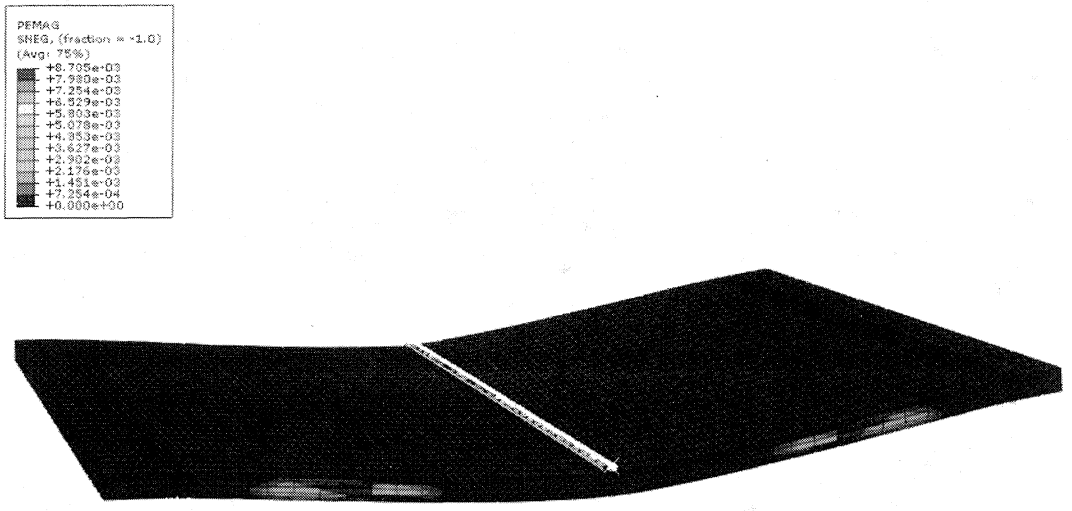

FIGURE 37: Plastic Strain for FEM drywall comparison test for 0.5" sandwich.

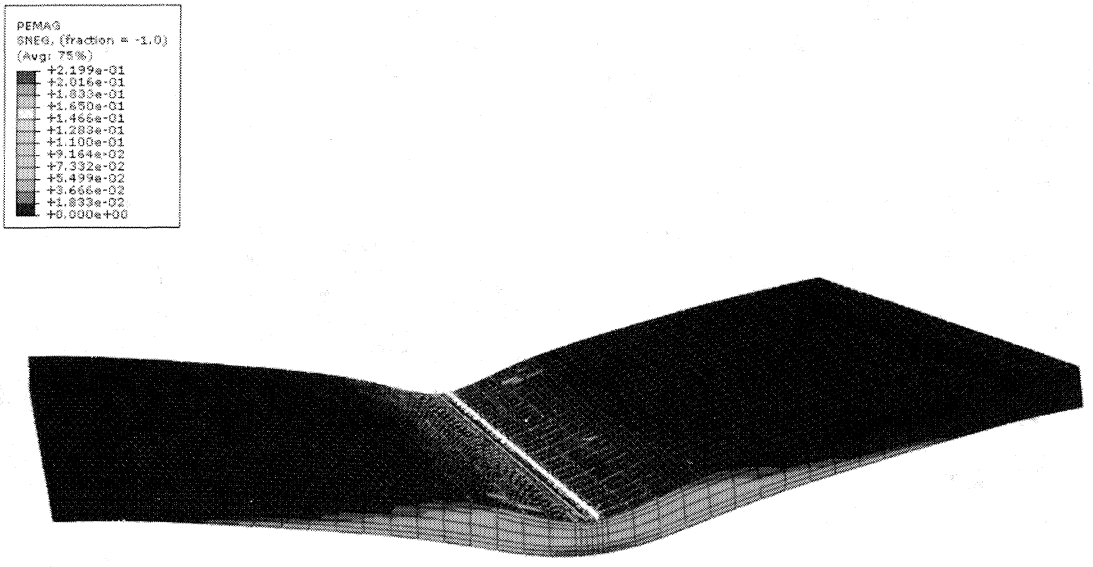

FIGURE 38: Plastic strain for FEM drywall comparison test for 0.75" sandwich.

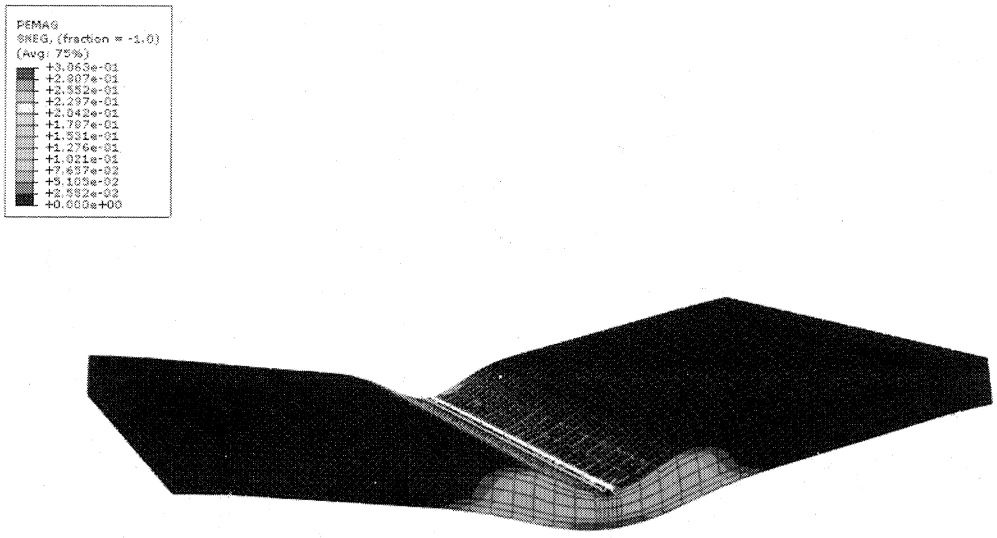

FIGURE 39: Plastic strain for FEM drywall comparison test for 1" sandwich.

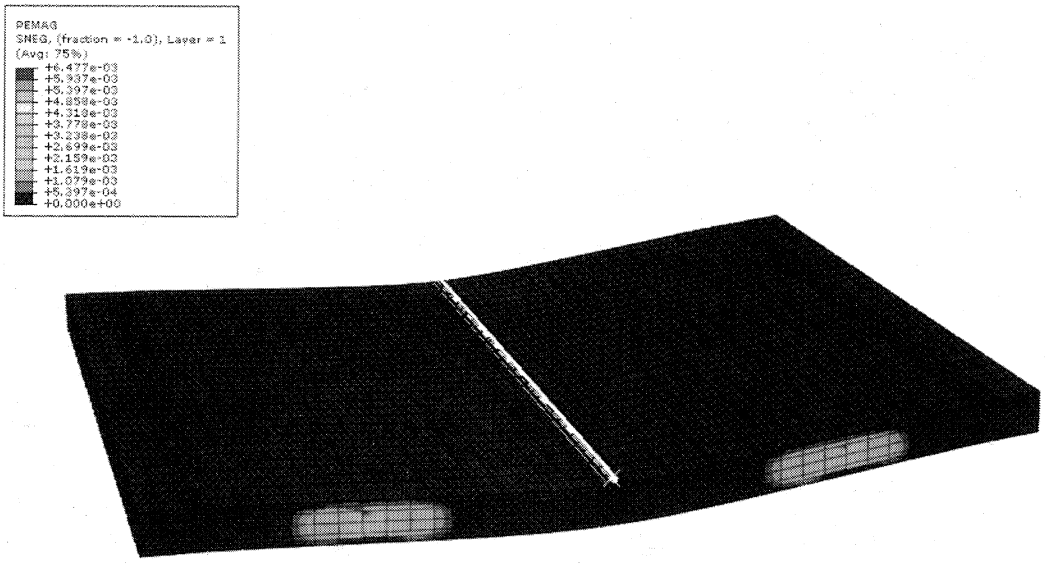

FIGURE 40: Plastic strain for FEM drywall comparison test for 1" sandwich with double layered face sheets.

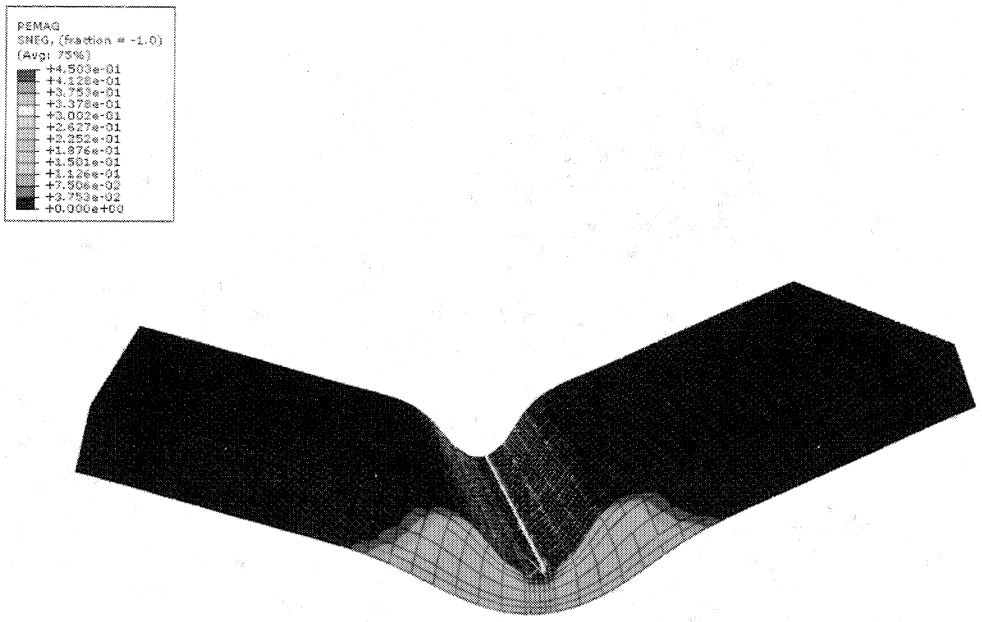

FIGURE 41: Plastic strain for FEM drywall comparison for 1.25" sandwich.

CHAPTER 6

CONCLUSIONS

Uniaxial compression tests showed that the addition of cooked rice hulls to the foam mixture created an increase in material strength over the virgin foam material. This illustrates a potential use for spent rice hulls at the end of their current use cycle, allowing the waste material to be used as both fuel in power plants and as reinforcement in a polymeric foam material. Additionally, castor oil is a viable substitute for petroleum-based chemicals during the foam production process.

The behavior of this sandwich material can be reasonably simulated by a model in Abaqus, utilizing the Hashin failure criteria and the Crushable Foam options to model damage in the laminate and foam, respectively. This model can then be used to compare the sandwich material to other materials with established testing procedures.

As a non-structural building panel, this sandwich biocomposite is about half the strength of an equally thick drywall panel. Thus, in conditions without severe space limitations, the sandwich panels are a structurally suitable replacement for drywall panels. By making use of waste rice hulls, hemp fiber, and other naturally renewable materials, the sandwich panels are also a more sustainable alternative to traditional gypsum drywall. In addition to this environmental advantage, the sandwich material is ductile in failure. This property is much preferred to the brittle nature of drywall, and could lead to more easily maintained interior walls in residential construction projects.

Further testing is required to determine the suitability of this novel material as a replacement for drywall in standard building applications. ASTM provides recommendations for thermal conductivity, combustibility, absorbance, nail pull resistance, humidified deflection, hardness, and impact resistance of drywall. These properties of the sandwich composite would need to be studied prior to its use in any construction projects. However, with this study showing a structural equivalence between the sandwich material and drywall, further study in this area both justified and recommended.

APPENDIX

SAMPLE ABAQUS INPUT FILE

This sample input file shows the various material properties, boundary conditions, and other interactions used in all the finalized models of this study. Most node, element, and set definitions are omitted for brevity. Additional comments are bolded and enclosed in brackets (**{comment here}**).

```
*Heading
** Job name: Sample_INP Model name: Model-1
** Generated by: Abaqus/CAE 6.10-1
*Preprint, echo=NO, model=NO, history=NO, contact=NO
**
** PARTS  {Node and element definitions are omitted for
brevity}
**
*Part, name=Core
*Element, type=C3D8R
** Section: Foam
*Solid Section, elset=_PickedSet2, material="Foam 5%
Cooked"
,
*End Part
**
*Part, name=FacePlate
*Element, type=S4R
** Section: Hemp
*Shell Section, elset=_PickedSet2, composite, offset=SPOS
0.06, 3, HFRP, 0., ply1
*End Part
**
*Part, name=Support
*End Part
**
**
** ASSEMBLY    {Element coordinates are omitted for
brevity}
**
*Assembly, name=Assembly
**
*Instance, name=Core-1, part=Core
*End Instance
**
*Instance, name=FacePlate-1, part=FacePlate
```

```
*End Instance
**
*Instance, name=FacePlate-2, part=FacePlate
*End Instance
**
*Instance, name=Support-1, part=Support
*Surface, type=CYLINDER, name=LoadRoller
START, 0.49749371855331, -0.0499999999999986
 CIRCL, -0.49749371855331, -0.0499999999999986,
0.,           0.
*End Instance
**
*Instance, name=Support-2, part=Support
*Surface, type=CYLINDER, name=Support2
START, 0.49749371855331, -0.0499999999999986
 CIRCL, -0.49749371855331, -0.0499999999999986,
0.,           0.
*End Instance
**
*Instance, name=Support-2-lin-2-1, part=Support
*Surface, type=CYLINDER, name=Support1
START, 0.49749371855331, -0.0499999999999986
 CIRCL, -0.49749371855331, -0.0499999999999986,
0.,           0.
*End Instance
**
*Node
      1,           2.,         1.38,         3.75
*Node
      2,           2.,         -0.5,          6.5
*Node
      3,           2.,         -0.5,           1.
```

{Set definitions are omitted for brevity}
{The following constraints assign the tie connections between the core and faceplates, and assign the 3 roller instances as rigid bodies}

```
** Constraint: BotTie
*Tie, name=BotTie, adjust=yes
MidLower, BotInner
** Constraint: Loader
*Rigid Body, ref node=_PickedSet32, analytical
surface=Support-1.LoadRoller
** Constraint: Support1Const
*Rigid Body, ref node=_PickedSet33, analytical
surface=Support-2-lin-2-1.Support1
** Constraint: Support2Const
```

```
*Rigid Body, ref node=_PickedSet34, analytical
surface=Support-2.Support2
** Constraint: TopTie
*Tie, name=TopTie, adjust=yes
MidUpper, InnerTop
*End Assembly
**
** MATERIALS
**
*Material, name="Foam 5% Cooked"
*Elastic
220., 0.01
*Crushable Foam
 1.1, 0.5
*Crushable Foam Hardening
 13.7198,        0.
 14.8792, 0.0115867
 16.0386, 0.0281702
 17.1981, 0.0433879
 17.5845, 0.0689483
  18.744, 0.0909953
 19.5169,  0.122994
 20.8696,  0.159187
  22.029,  0.203088
 23.5749,  0.241134
 25.1208,  0.281912
 26.4734,  0.319471
 28.4058,  0.353029
 30.3382,  0.386587
 32.2705,  0.417413
 34.5894,   0.45058
 36.9082,  0.486479
 39.4203,  0.517402
 42.3188,  0.542471
 45.2174,  0.566174
 48.5024,   0.58812
 51.5942,   0.61231
 55.0725,   0.62928
 59.3237,  0.649566
 63.1884,  0.674341
 68.0193,  0.686529
  72.657,  0.696863
 76.9082,  0.704856
 81.7391,  0.712946
 86.3768,  0.717817
 91.5942,  0.724151
```

```
 97.1981,   0.72463
 101.449,  0.731257
*Material, name=HFRP
*Damage Initiation, criterion=HASHIN
7095.,  1000.,  7095.,  1000., 583.33,   300.
*Elastic, type=LAMINA
338833.,338833.,   0.27, 21875.,  8750.,  8750.
**
** INTERACTION PROPERTIES
**
*Surface Interaction, name=RollerIntProp
1.,
*Friction, slip tolerance=0.005
 0.001,
*Surface Behavior, pressure-overclosure=HARD
**
** BOUNDARY CONDITIONS
**
** Name: Load Roller Type: Displacement/Rotation
*Boundary {This BC fixes all motion of the loading roller
except vertical translation}
_PickedSet36, 1, 1
_PickedSet36, 3, 3
_PickedSet36, 4, 4
_PickedSet36, 5, 5
_PickedSet36, 6, 6
** Name: Support Rollers Type: Displacement/Rotation
*Boundary {This BC fixes all motion of the support rollers}
_PickedSet40, 1, 1
_PickedSet40, 2, 2
_PickedSet40, 3, 3
_PickedSet40, 4, 4
_PickedSet40, 5, 5
_PickedSet40, 6, 6
** Name: Z-Con Type: Displacement/Rotation
*Boundary {This BC constrains the centerline on the top
face of the beam}
Z-Rest, 1, 1
Z-Rest, 3, 3
**
** INTERACTIONS
**
** Interaction: LoaderInt
*Contact Pair, interaction=RollerIntProp, type=SURFACE TO
SURFACE, tracking=STATE
TopSurf, Support-1.LoadRoller
```

```
** Interaction: Sup1Int
*Contact Pair, interaction=RollerIntProp, type=SURFACE TO
SURFACE, tracking=STATE
BotSurf, Support-2-lin-2-1.Support1
** Interaction: Sup2Int
*Contact Pair, interaction=RollerIntProp, type=SURFACE TO
SURFACE, tracking=STATE
BotSurf, Support-2.Support2
** ----------------------------------------------------
--------
**
** STEP: Load
**
*Step, name=Load, nlgeom=YES, inc=1000, unsymm=YES
*Static, riks  {This includes the test stopping point of 2
inches}
0.01, 1., 1e-15, , , LoadRP, 2, -2.
**
** BOUNDARY CONDITIONS
**
** Name: Load Type: Displacement/Rotation
*Boundary {This applies a 1 inch displacement for every 1
step time}
_PickedSet37, 2, 2, -1.
**
** OUTPUT REQUESTS
**
*Restart, write, frequency=0
**
** FIELD OUTPUT: F-Output-1
**
*Output, field
*Node Output
CF, RF, TF, U
*Element Output, directions=YES
LE, PE, PEEQ, PEMAG, S
*Contact Output
CDISP, CSTRESS
**
** HISTORY OUTPUT: H-Output-1
**
*Output, history    {This outputs XY data for the load-
displacement graph}
*Node Output, nset=LoadRP
RF2, RT, U2
*End Step
```

REFERENCES

REFERENCES

ASTM International. (2008a). "Standard Test Methods for Flexible Cellular Materials Made From Olefin Polymers." D3575-08, West Conshohocken, PA.

ASTM International. (2008b). "Standard Test Method for Tensile Properties of Polymer Matrix Composite Materials." D3039-08, West Conshohocken, PA.

ASTM International. (2012a). "Standard Practice for Determining Sandwich Beam Flexural and Shear Stiffness." D7250-06, West Conshohocken, PA.

ASTM International. (2012b). "Standard Test Methods for Physical Testing of Gypsum Panel Products." C473-12, West Conshohocken, PA.

ASTM International. (2013). "Standard Specification for Gypsum Board." C1396-13, West Conshohocken, PA.

Borsellino, C., Calabrese, L., and Valenza, A. (2004). "Experimental and numerical evaluation of sandwich composite structures." *Compos. Sci. Technol.*, 64(10-11), 1709–1715.

Burgueño, R., Quagliata, M. J., Mehta, G. M., Mohanty, A. K., Misra, M., and Drzal, L. T. (2005). "Sustainable Cellular Biocomposites from Natural Fibers and Unsaturated Polyester Resin for Housing Panel Applications." *J. Polym. Environ.*, 13(2), 139–149.

Dassault Systèmes. (2010). "Abaqus Documentation." Release 6.10, Providence, RI.

Faruk, O., Bledzki, A. K., Fink, H.-P., and Sain, M. (2012). "Biocomposites reinforced with natural fibers: 2000–2010." *Prog. Polym. Sci.*, Elsevier, 37(11), 1552–1596.

Fereidoon, A., and Taheri, S. A. (2012). "Using finite element method to analyze the effect of microstructure on energy absorption properties of open cell polymeric foams." *J. Cell. Plast.*, 48(3), 257–270.

Flores-Johnson, E. A., and Li, Q. M. (2012). "Structural behaviour of composite sandwich panels with plain and fibre-reinforced foamed concrete cores and corrugated steel faces." *Compos. Struct.*, 94(5), 1555–1563.

Hassan, N. M., and Batra, R. C. (2008). "Modeling damage in polymeric composites." *Compos. Part B Eng.*, 39(1), 66–82.

Ivañez, I., Santiuste, C., and Sanchez-Saez, S. (2010). "FEM analysis of dynamic flexural behaviour of composite sandwich beams with foam core." *Compos. Struct.*, Elsevier, 92(9), 2285–2291.

Jawaid, M., and Abdul Khalil, H. P. S. (2011). "Cellulosic/synthetic fibre reinforced polymer hybrid composites: A review." *Carbohydr. Polym.*, Elsevier., 86(1), 1–18.

John, M., and Thomas, S. (2008). "Biofibres and biocomposites." *Carbohydr. Polym.*, 71(3), 343–364.

Kabir, M. M., Wang, H., Lau, K. T., Cardona, F., and Aravinthan, T. (2012). "Mechanical properties of chemically-treated hemp fibre reinforced sandwich composites." *Compos. Part B Eng.*, Elsevier, 43(2), 159–169.

Kreja, I. (2011). "A literature review on computational models for laminated composite and sandwich panels." *Cent. Eur. J. Eng.*, 1, 1–39.

La Mantia, F. P., and Morreale, M. (2011). "Green composites: A brief review." *Compos. Part A Appl. Sci. Manuf.*, Elsevier, 42(6), 579–588.

Li, Q. M., Mines, R. a. W., and Birch, R. S. (2000). "The crush behaviour of Rohacell-51WF structural foam." *Int. J. Solids Struct.*, 37(43), 6321–6341.

Lim, T. S., Lee, C. S., and Lee, D. G. (2004). "Failure Modes of Foam Core Sandwich Beams under Static and Impact Loads." *J. Compos. Mater.*, 38(18), 1639–1662.

Mamalis, A. G., Spentzas, K. N., Manolakos, D. E., Ioannidis, M. B., and Papapostolou, D. P. (2008). "Experimental investigation of the collapse modes and the main crushing characteristics of composite sandwich panels subjected to flexural loading." *Int. J. Crashworthiness*, 13(4), 349–362.

Mendez, S., Aungyong, L., Chan, K., and Ko, Y. (2013). "Fabrication of Polyurethane-Based Foams with Incorporated 'Waste' Glycerol from Tranesterification Synthesis and 'Waste' Agricultural Residues (Chopped Rice Hull Fibers)." 1–8.

Mendez, S., and Ko, Y. (2013). *Sustainable Green Building Materials: Fabrication of Biofoam/Hemp Boards from Waste Sources.* 1–8.

Mines, R. A. ., and Alias, A. (2002). "Numerical simulation of the progressive collapse of polymer composite sandwich beams under static loading." *Compos. Part A Appl. Sci. Manuf.*, 33(1), 11–26.

Mines, R. A. W., and Jones, N. (1995). "Approximate elastic-plastic analysis of the static and impact behaviour of polymer composite sandwich beams." *Composites*, 26(12), 803–814.

Rizov, V. (2008). "Failure behavior of composite sandwich structures under local loading." *Arch. Appl. Mech.*, 79(3), 205–212.

Saha, M. C., Kabir, M. E., and Jeelani, S. (2008). "Enhancement in thermal and mechanical properties of polyurethane foam infused with nanoparticles." *Mater. Sci. Eng. A*, 479(1-2), 213–222.

Steeves, C. A., and Fleck, N. A. (2004a). "Collapse mechanisms of sandwich beams with composite faces and a foam core, loaded in three-point bending. Part I: analytical models and minimum weight design." *Int. J. Mech. Sci.*, 46(4), 561–583.

Steeves, C. A., and Fleck, N. A. (2004b). "Collapse mechanisms of sandwich beams with composite faces and a foam core, loaded in three-point bending. Part II: experimental investigation and numerical modelling." *Int. J. Mech. Sci.*, 46(4), 585–608.

Tagarielli, V. L., Fleck, N. a., and Deshpande, V. S. (2004). "Collapse of clamped and simply supported composite sandwich beams in three-point bending." *Compos. Part B Eng.*, 35(6-8), 523–534.

Zhang, J., Lin, Z., Wong, A., and Kikuchi, N. (1997). "Constitutive modeling and material characterization of polymeric foams." *J. Eng. Mater. Technol.*, 119, 284–291.